Journal of Inflammation Research

Dovepress
Taylor & Francis Group

Open Access Full Text Article

ORIGINAL RESEARCH

Coix Seed Oil Alleviates DSS-Induced Ulcerative Colitis via Intestinal Barrier Repair and Ferroptosis Regulation

Yi-Xuan Zeng*, Ni-Ren Li*, Bing-Ying Deng*, Yu-Feng Gu, Si-Fan Lu, Yi Liu

Traditional Chinese Pharmacological Laboratory, Guangdong Provincial Key Laboratory of Chinese Medicine Pharmaceutics, Guangdong Basic Research Center of Excellence for Integrated Traditional and Western Medicine for Qingzhi Diseases, School of Traditional Chinese Medicine, Southern Medical University, Guangzhou, 510515, People's Republic of China

*These authors contributed equally to this work

Correspondence: Yi Liu, Email liuyi099@163.com

Background: Ulcerative colitis is a chronic intestinal disease linked to intestinal barrier damage, ferroptosis and dysbiosis. *Coix lacryma-jobi* is a natural food with food-medicine homology, whose seed-derived oil (Coix seed oil, CSO) has been shown anti-inflammatory activity in vitro. Here, the effects and mechanisms of CSO on ulcerative colitis (UC) in vivo are systematically investigated.

Methods: Firstly, the UC mice was replicated by 3% DSS, and assessed the efficacy of CSO by observing the fecal occult blood, colon length, DAI score and pathological histomorphological changes of colon tissues. The anti-inflammatory and barrier-protective effects of CSO were observed by AB staining and qRT-PCR. Secondly, the biological targets of CSO were obtained from TCMSP database and Swiss Target Prediction database, ferroptosis targets were downloaded from FerrDb platform, and UC-related disease targets were obtained from GEO database, and the intersection of the above three was taken to obtain "CSO-UC-Ferroptosis" intersection targets, which were analysed by GO and KEGG enrichment, GSEA analysis, and immune cell infiltration and validation. Finally, the core genes of "CSO-UC-Ferroptosis" were molecular docking with the potential active components of CSO. In order to further verify the effect of CSO on ferroptosis, the GPX4 agonist RSL-3 was used to stimulate mice in vivo, and the levels of Iron, MDA and SOD were measured, and immunohistochemistry was used to detect the effects of tight junction proteins and the "CSO-UC-Ferroptosis" core protein in mice. Besides, the effect of CSO was further evaluated by observing the intercellular junctions of the colon tissues of each group under electron microscope. In addition, 16sRNA sequencing was performed on the intestinal contents of the mice to observe the effects of CSO on the intestinal flora of UC mice.

Results: CSO improved physiological parameters, reduced inflammation response and intestinal barrier damage, regulated ferroptosis, and restored gut microbiota balance in UC mice. Bioinformatics results showed that *G6PD, ABCC1* were core targets at the intersection of CSO, UC and ferroptosis, which also demonstrated the similar expression of the core genes in DSS-induced UC mice models in vivo.

Conclusion: Our findings demonstrate for the first time that CSO ameliorated UC by regulating intestinal barrier damage, ferroptosis and the gut microbiota in DSS-induced mice, suggesting that CSO as a promising candidate for UC treatment and warranting further investigation.

Keywords: coix seed oil, ulcerative colitis, intestinal barrier, ferroptosis, network pharmacology, gut microbiota

Introduction

With the rise of industrialization and changes in people's dietary structures, the incidence of ulcerative colitis (UC) is still increasing year by year around the world.[1] As a chronic inflammatory bowel disease, UC patients are mostly characterized with persistent or recurrent abdominal pain, diarrhea, mucus-blood stools and weight loss,[2] and the course of UC may also be complicated by gastrointestinal hemorrhage, perforation, toxic megacolon, cancer and so forth, seriously

Received: 7 November 2024
Accepted: 5 February 2025
Published: 20 February 2025

affected the productivity and life of the sufferers.[3] Despite advances in pharmacological and surgical interventions, many patients experience relapses and long-term side effects, necessitating safer, cost-effective alternatives.[4,5]

The pathogenesis of UC is closely related to oxidative stress (OS) which lead to an imbalance in the homeostasis of intracellular iron ion metabolism, exacerbating lipid peroxidation and GSH depletion, which in turn triggers excessive ferroptosis.[6,7] Ferroptosis, a type of programmed cell death driven by oxidative stress, contributes to persistent colonic damage in UC.[8,9] Targeting this pathway may offer novel therapeutic opportunities.[10,11] Besides, UC was also regarded as highly associated with dysbiotic expansion of gut pathogenic microbes.[12] Dysbiosis, characterized by a decrease in beneficial bacteria and an increase in pathogenic species, exacerbates intestinal inflammation and barrier dysfunction, making microbiota modulation a key therapeutic strategy. When IBD occurs, certain specific bacterial species tend to grow at high levels in the affected population.[13] The active components and metabolites of these bacteria have been found to promote disease progression by disrupting the intestinal microbiota and impairing intestinal barrier function, and the inflamed intestinal microenvironment may further increase the level of OS in the gut, potentially leading to worsening of the inflammation or transition to cancer, such as inflammatory-associated colorectal cancer.[14,15] Therefore, specific inhibition of the abundance of dangerous intestinal bacteria and repair of the intestinal barrier damage may greatly alleviate the symptoms of colitis.

As a kind of traditional Chinese medicine (TCM) derived with food-medicine homology, *Coix lacryma-jobi* has been widely used in East Asia for over 2000 years. CSO, a mixture of lipids and fat-soluble functional ingredients extracted derived from *Coix lacryma-jobi*, has demonstrated efficacy in models of inflammation and cancer through mechanisms such as mitochondrial modulation and immune regulation, widely used in clinical breast cancer, primary non-small cell lung cancer and primary liver cancer.[16,17] Now, CSO may also implicated in UC. Recent studies have shown that immune response is involved in the development of inflammatory bowel disease, and UC is closely related to intestinal immunity.[18,19] Intestinal inflammation exacerbates intestinal barrier damage, which is continuously disrupted by inflammatory mediators, and this inflammatory cascade subsequently leads to the chronicity of UC.[20] Some research have been demonstrated that active ingredients of TCM may inhibit inflammatory responses and OS during UC by interfering with iron metabolism, correcting lipid metabolism and peroxidation accumulation, and regulating processes such as GSH and glutathione peroxidase 4 (GPX4).[21,22] CSO has been found to induce apoptosis in human pancreatic cancer cells by regulating mitochondrial damage through PTEN/PI3K/AKT pathway.[23] The consumption of CSO could affect the gut microbiota and the peripheral lymphocyte subset profiles of healthy males.[24] Hu has found that coixol exerts anti-inflammatory effects by inhibiting the activation of NF-κB, MAPKs pathways in RAW 264.7 cells.[25] However, the protective effects and mechanisms of CSO on UC have rarely been reported. Therefore, this study aims to explore the role of CSO in alleviating UC inflammation and barrier protection by alleviating oxidative stress as well as ferroptosis and regulating intestinal flora, providing new possible alternatives for clinical treatment.

Materials and Methods

Chemicals and Reagents

Dextran sulfate sodium salt was bought from Macklin (Lot. No. C13298093, Shanghai, China). Coix seed oil was obtained from Weikeqi (Lot. No.03187, Chengdu, China). Mesalazine was purchased from Kuihua (Lot. No.230518, Heilongjiang, China). Ferrostatin-1 was bought from APE Bio (Lot. No. A4371). RSL-3 (Lot. No. R302648), Soybean oil (Lot. No. S110245) was from Aladdin (Shanghai, China). The antibody for Claudin 1Ab (Lot. No. AF0127) was from Affinity (Melbourne, Australia). Antibodies for E-cadherin (Lot. No. 3195T), ZO-1 (Lot. No. 91131T), GAPDH (Lot. No. 5174T) and β-actin (Lot. No. 8457T) were aquired from Cell Signaling Technology (Boston, MA, USA). Anti-GPX4 antibody (Lot. No. H680019015), MRP1 (Lot. No.1704–56), AKR1C1 (Lot. No.1512–11), G6PD (Lot. No.1706–7), PARP1 (Lot. No. ET1608-56) was purchased from Huabio (Hangzhou, China). BCA protein assay kit (Lot. No. P0012S) and RIPA lysate buffer (Lot. No. P0013B) from beyotime (Shanghai, China), phosphate-buffered saline (PBS, Lot. No. BL601A) from Biosharp (Hefei, China) and enhanced chemiluminescence (ECL) from NCM Biotech (Lot. No. P10100) were purchased from Saiguobio (Guangzhou, China). Polyvinylidene difluoride (PVDF) membranes (Lot. No.0000155412) was obtained from Merck Millipore Ltd. (Billerica, MA, USA). AG RNAex Pro Reagent (Lot. No. AG21102), Evo M-MLV reverse transcription kit II (Lot. No. AG11711) were bought from Aikorui (Changsha, China).

Development of the Animal Model and Ethics Statement

56 SPF grade C57BL/6J mice (males, 7 weeks old, weighing 20–22 g) were purchased from the Experimental Animal Center of Southern Medical University (license number: SCXK (Yue) 2021–0041). During the experiment, all mice were kept in animal chambers under standard conditions (raised at 22 ± 2 °C with a 12/12 hour cycle (light/dark)). Animal welfare and experimental procedures were carried out in strict accordance with the Guidelines for the Management and Use of Experimental Animals and were approved by the Animal Ethics Committee and the Animal Protection and Utilization Committee of Institute of Southern Medical University. The approval is SMUL202311042. All mice were strictly controlled under the same animal housing conditions for all experimental manipulations.

As in previous experiments, 3% DSS solution was used to construct the experimental UC model.[26] The mice were fed with water containing DSS over a period of Day 1 to Day 8, then were fed with ordinary drinking water from Day 9 to Day 11. After modeling, the mice were killed, and the colon tissues of the mice were removed. Part of the colon was used to extract protein and RNA for follow-up experiments, and part of the colon was fixed by 4% paraformaldehyde, dehydrated, embedded, and sliced for pathological experiments.

Disease Activity Index (DAI)

Throughout the duration of the experiment, the general condition, water intake, weight, and stool characteristics of the mice were observed every day, and the detection of occult blood in stool of them was observed by benzidine and 3% perhydrol at Day 5. After the modeling, the percentage of daily weight of the animals was calculated. The DAI scores were calculated as the sum of the weight loss rate score, fecal traits score, and intestinal bleeding score.

Histopathological Examination and Histological Index (HI) of Colon Tissue

On Day 11, all groups of the mice were killed, and the colon tissue was immediately removed and fixed with 4% (w/v) paraformaldehyde solution, paraffin embedded, cut into 4 μM section, and finally stained with hematoxylin and eosin (H&E) for histopathological examination, then calculate the sum of the histological index of H&E stained colon sections.

mRNA Extraction and Real-Time qRT-PCR

Total RNA was extracted from colon tissue using Trizol reagent. After quantification using an ultra micro spectrophotometer, cDNA was synthesized using the Evo M-MLV reverse transcription kit II. Then, the qRT-PCR reaction was performed using the reagent kit from Aikorui Biotechnology, and cDNA was amplified using the real-time PCR system, Thermo Fisher Scientific Quantum Studio 5 (Waltham, MA, USA). The PCR cycle conditions are: 95 °C for 30 seconds for pre-denaturation; 95 °C for 10 seconds for denaturation; 60 °C for 40 seconds for annealing and extension; amplify for 40 cycles. The total reaction volume is 20 μL. The qRT-PCR primers are shown in Table 1.

Acquisition of Biological Targets of CSO and Ferroptosis Targets

CSO was searched from Traditional Chinese Medicine Systems Pharmacology database and analysis platform (https://old.tcmsp-e.com/), Swiss Target Prediction database (http://swisstargetprediction.ch) combined with literature reviews to obtain the total corresponding targets. Ferroptosis-related genes (FRGs) were obtained from the FerrDb platform (http://zhounan.org/ferrdb) by downloading the driver, marker and suppressor datasets.

Acquisition of the GEO Database Disease Set

The UC patients data used in this study were obtained from the GEO database (https://www.ncbi.nlm.nih.gov/GEO/). In the GEO database, we entered "Ulcerative colitis" as the keyword, and filtered the criteria: "Homo sapiens", "Series", "Expression profiling by array", "Homo sapiens", "Series", "Expression profiling by array", and dataset requirements: (1) The total sample size is greater than 20; (2) Contain untreated UC group and healthy group; (3) Select two database as test group and validation group. The GEO database was searched according to the above requirements to obtain GSE87473, GSE206285. The GSE87473, GSE206285 datasets were standardized using the "limma" R package, including annotation and correction.

Table 1 Primer Sequence of Mouse

Genes	Primer Sequence (5'→3')
NF-κB-For	ATGGCAGACGATGATCCCTAC
NF-κB-Rev	TGTTGACAGTGGTATTTCTGGTG
TNF-α-For	TCACGCTCCATAAGACCCAG
TNF-α-Rev	GATGTGCAAAGACACCTGGC
IL-6-For	ACTCACCTCTTCAGAACGAATTG
IL-6-Rev	CCATCTTTGGAAGGTTCAGGTTG
IL-1β-For	CGTGAAGTGAACGTGGTGGA
IL-1β-Rev	GTACGAGATGTGGAGACGTGG
Occludin-For	ATAATGGGAGTGAACCCGAC
Occludin-Rev	CTCCTGGGGATCAACCAC
Claudin-For	GCAAGGTGTATGAATCTGTGCT
Claudin-Rev	GTCAAGGTAACAAAGAGTGCCA
ZO-1-For	GCCGCTAAGAGCACAGCAA
ZO-1-Rev	GCCCTCCTTTTAACACATCAGA
β-actin-For	GTGACGTTGACATCCGTAAAG
β-actin-Rev	GCCGGACTCATCGTACTCC

Screening of Differentially Expressed Genes for "CSO-UC-Ferroptosis" Intersection Targets

The intersection of CSO-related genes, UC-related genes and FRGs was identified using the Venny 2.1.0 website to obtain common targets of action. Subsequently, the "limma" R language package was utilized to extract the DEGs from this intersection within the test set GSE206285. The p value < 0.05 was set as the threshold for differential gene expression for the output and analysis results. Finally, heatmaps was generated using the "pheatmap" R language package.

GO Enrichment and KEGG Signaling Pathway Analysis of "CSO-UC-Ferroptosis" Intersection Targets

The intersecting genes were K-plotted by R packages such as "clusterProfiler",[27] "enrichplot", "org.Hs.eg.db", "ggplot2",[28] among others, to analyze the KEGG and GO enrichment of intersecting genes, and to display the top 30 pathways in the form of bubble plots and bar graphs. GO and KEGG enrichment analysis was performed using the enrich KEGG function, which by default uses the Benjamini–Hochberg method with the FDR (False Discovery Rate) correction to calculate the q-value.

Screening of Genes Characterized by "CSO-UC-Ferroptosis" by ROC Curve Assessment

To assess the diagnostic efficacy of UC-characteristic diagnostic gene markers associated with ferroptosis for UC, array data from the test set GSE206285, including 21 control samples and 87 UC patient samples, were used to plot the receiver operating characteristic (ROC) curves based on their expression of the relevant gene markers.[29] By constructing a logistic regression model, all genes from the integrated intersection of interest were combined, and subsequently, model scoring was performed. The diagnostic efficacy was quantitatively assessed by calculating the Area Under Curve (AUC) of each ROC curve, which was plotted using the "pROC" and "glmnet" packages in R.[30] The closer the AUC value is to 1, the higher the diagnostic efficacy.

Enrichment of GSEA to Analyze "CSO-UC-Ferroptosis" Cross-Targets

In order to further investigate the biological processes associated with the identified biomarkers, this study continued with Gene Set Enrichment Analysis (GSEA) of the targeted biomarkers.[31] First, the gene sets "c5.go.symbols" and "c2.

cp.kegg.symbols" were downloaded from the molecular characterization database MSigDB, and these were analyzed by GSEA algorithms to explore the biological processes and pathways that may be associated with the markers. Among the tools used were the R packages "limma", "clusterProfiler",[27] "enrichplot", "org.Hs.eg.db", "GSEABase", "reshape2".[32] A corrected p-value of <0.05 was considered statistically significant for the enriched results.

Correlation of the "CSO-UC-Ferroptosis" Intersection Target With the Level of Immune Cell Infiltration

CIBERSORT reverse convolution was applied to assess the percentage of 22 immune cells in the samples from the GSE206285 dataset. The simulations were calculated 1000 times, and the data with $P<0.05$ were analyzed to determine the percentage of immune cells in different samples. Subsequently, the "limma" was applied, "tidyverse",[33] "ggplot2", and other R packages were applied to analyze the correlation between characterized genes and immune cells, and to generate correlation heatmaps.

Validation of Biomarkers Associated With "CSO-UC-Ferroptosis"

Using the "limma" and "ggpubr" R packages, the data from the validation set GSE87473 were normalized and used for differential gene expression analysis. The box plots of the characterized genes were generated to verify whether the aforementioned FRGs were also significantly different in the validation set.

Molecular Docking of the Core Targets for "CSO-UC-Ferroptosis"

In order to confirm the binding potential of CSO, we targeted disease-related proteins and applied molecular docking techniques to further predict the full potential therapeutic effect of the drug.[34] The specific methods were as follows: the active monomer components of the compound were downloaded from the TCMSP database, and the target protein structures were downloaded from the UniProt database (https://www.uniprot.org/) and the PDB database (https://www.rcsb.org/). Then, the above monomer and protein files were processed and converted to PDBQT format using AutoDock Tools 1.5.7 software. Ligand–molecule interactions were docked by AutoDock vina, and binding energy data were obtained. Finally, the docking results were visualized using Pymol.

Immunohistochemistry

The expression of E-cadherin, ZO-1, Claudin, GPX4, MRP1, G6PD was detected according to a method described them elsewhere. In a nutshell, colon paraffin sections were antigen repaired, sealed with serum and added the primary antibody, then incubated overnight in a refrigerator at 4 °C. The second day, the colon tissues were washed with PBS and incubated with poly-HRP antirabbit IgG at room temperature for 30 minutes. After incubation, add DAB colorimetric solution dropwise to the tissue for staining. Finally, all samples were detected and photographed using a slicing scanner. Image Pro Plus 6.0 software is used for data analysis.

Gut Microbiota Analysis

Colon contents DNA from mice were extracted to amplify the 16S rRNA gene (V3-V4 region). The amplification utilized primers 338F (5'- ACTCCTACGGGAGGCAGCAG – 3') and 806R (5'- GGACTACHVGGGTWTCTAAT – 3'). PCR products were sequenced using the Illumina MiSeq PE300 system. The raw reads obtained from MiSeq sequencing were initially assembled based on overlapping sequences, with strict quality control, baseline microbiota control and filtering applied. A total of 1956328 optimised sequences with 2208856352 optimised base pairs (bp) were obtained from this sequencing, with an average sequence length of 1427 bp. Operational Taxonomic Unit (OTU) clustering analysis and species taxonomy analysis were performed. Subsequent bioinformatics analyses were conducted using the cloud service platform provided by Shanghai Majorbio Bio-pharm Technology Co., Ltd.

Statistical Analysis

Statistical analysis was conducted using GraphPad Prism Software version 8.0 (GraphPad Software Inc.La Jolla, California, USA) for statistical analysis and mapping. All data are expressed as mean ± standard deviation (SD). The statistical analysis methods include one-way analysis of variance (ANOVA) to compare continuous data between multiple groups, and the Tukey method was used for multiple comparisons. In this study, $P < 0.05$ indicates a statistically significant difference. Among them, $*P < 0.05$, $**P< 0.01$, $***P < 0.001$, ns had no significant difference.

Results

CSO Improved Physiological Indexes and Attenuated Histopathological Characteristics in DSS-Induced UC Mice

In this study, 3% DSS-induced UC mouse model was successfully established and applied to explore the protective effect of CSO against UC (Figure 1A). During this experiment, typical pathological features of UC were observed in DSS-induced mice, including reduced appetite, weak movements, diarrhea, and blood in stool. Compared with the control group, DSS-induced mice showed decreased body weight (Figure 1B), shortened colon length (Figure 1C and D), and increased DAI scores (Figure 1G). After CSO and mesalazine treatments, these phenomena were effectively recovered compared with DSS group. At the end of experiment, the body weights in the DSS+CSO-L and DSS+CSO-H groups were much higher than those in the DSS group, suggesting that CSO administration at 12.5 and 50 mg/kg/d may had no toxicity on mice. It is clear that the length of the colon in DSS-induced colitis mice was dramatically shorter than that of control mice, where DSS+Mesalazine, DSS+CSO-L and DSS+CSO-H groups could significantly inhibit colon shortening.

H&E staining showed severe damage in the colon tissues of DSS-induced mice, such as mucosal ulceration, crypt destruction, and inflammatory cell infiltration (Figure 1E). And these pathological characteristics were markedly alleviated by CSO and mesalazine (Figure 1F), with CSO at the dose of 50mg/kg/d being more effective. These results showed that CSO treatment could improve the physiological indexes and attenuate histopathological characteristics in DSS-induced UC mice.

CSO Reduced Inflammatory Biomarkers and Alleviated DSS-Induced Intestinal Injury via Improving Intestinal Barrier Injury in UC Mice

The contents of pro-inflammatory cytokines in colon tissues were measured to evaluate the mitigation of CSO on the inflammation in UC mice. Consistently, the levels of NF-κB, TNF-α, IL-1β and IL-6 in UC mice were remarkably higher than those in control group (Figure 2A–D). Notably, the levels of these cytokines were downregulated by CSO, significantly lower than that in the DSS group. According to the results, CSO administration at 50 mg/kg showed more effective activity.

Mechanical barriers, one of the intestinal barrier components, contain tight junction (TJ) proteins, and alterations in TJ proteins can lead to the creation of intestinal barrier clefts.[35] Cuprocytes in the intestinal epithelium play a key role in intestinal immunity by secreting mucin to form a mucus layer attached to the epithelial surface to isolate and control colonisation and invasion of intestinal microbes. Firstly, the alcian staining was used to detect the number of cuprocytes, which showed a clear decrease in the DSS group. Specifically, the goblet cell numbers and shapes were dramatically recovered to a nearly normal level after mesalazine and CSO administration (Figure 2E). The low expression of TJ proteins is the crucial point in triggering intestinal barrier damage, which promotes inflammatory outbreaks.[36] According to the qRT-PCR results, the levels of ZO-1, occludin and claudin 1Ab were notably decreased in UC mice compared to the control mice, which were remarkably reversed by mesalazine and CSO at 50 mg/kg (Figure 2F–H). These results revealed that CSO possess with good effects on anti-inflammatory and the intestinal barrier repairing.

Network Pharmacology and Bioinformatics Analysis Among "CSO-UC-Ferroptosis"

Screening of Candidate Targets

The 10 compounds of CSO and 378 related target genes from databases were collected. Four hundred and seventy-eight ferroptosis-related genes (FRGs) were obtained from the FerrDb platform. To identify the UC-related targets, the GSE206285-based microarray GPL13158 data set from GEO database was downloaded and later served as a test set.

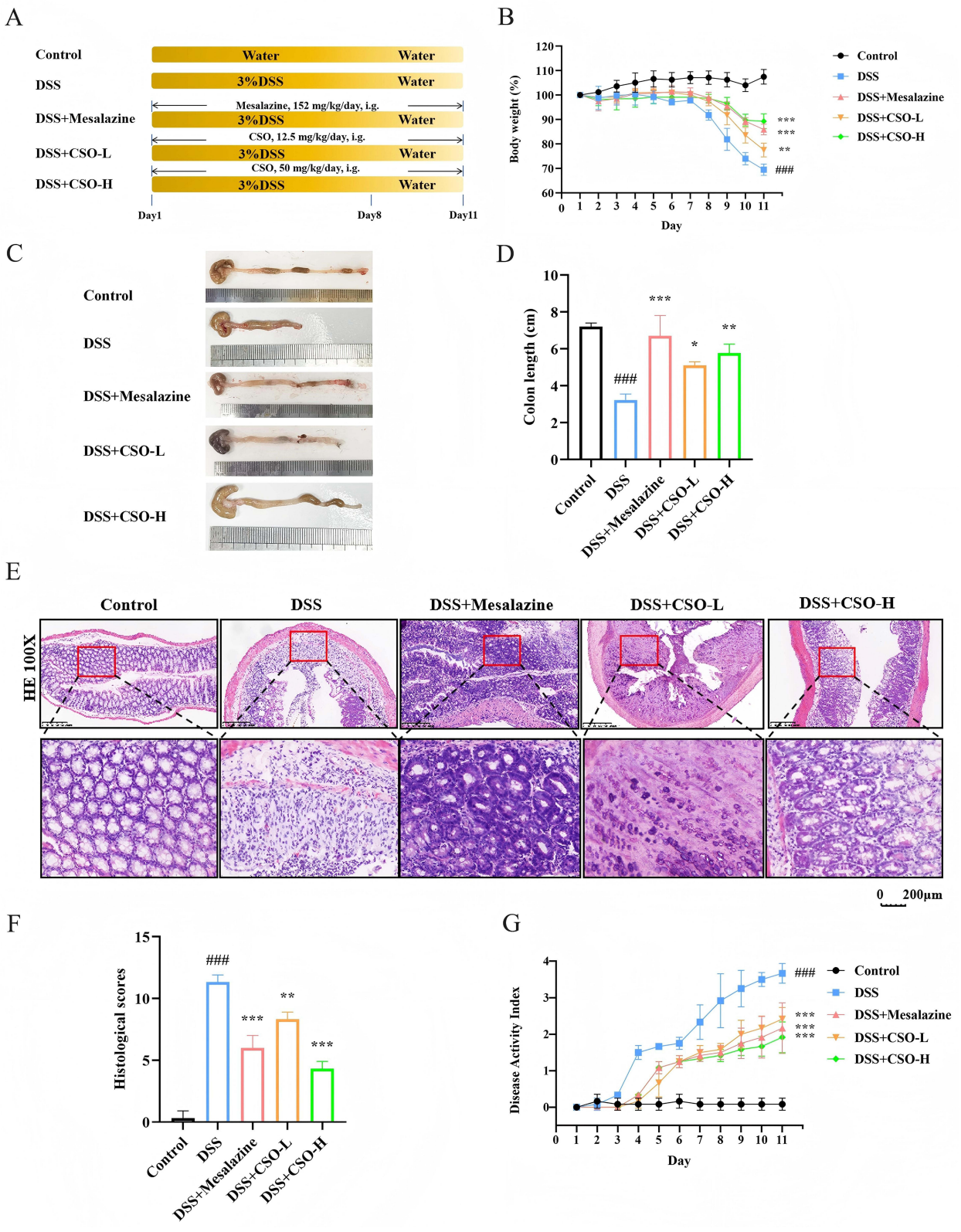

Figure 1 Alleviation of CSO in DSS-induced mice. (**A**) Experimental graph of the establishment of UC mice and drugs interventions; (**B**) Percentage change in body weight of mice; (**C**) Representative photographs of colons; (**D**) Comparison of colon length among the groups; (**E**) HE staining of colon tissues (magnification, 100×; scale bar, 200 μm); (**F**) Histopathological scoring of colon tissues; (**G**) Assessment of disease activity index. n=3-6. The data were presented as the means ± SEM. $^{###}P < 0.001$, vs Control group; $^{*}P < 0.05$, $^{**}P < 0.01$ and $^{***}P < 0.001$ vs DSS group.

https://doi.org/10.2147/JIR.S501745

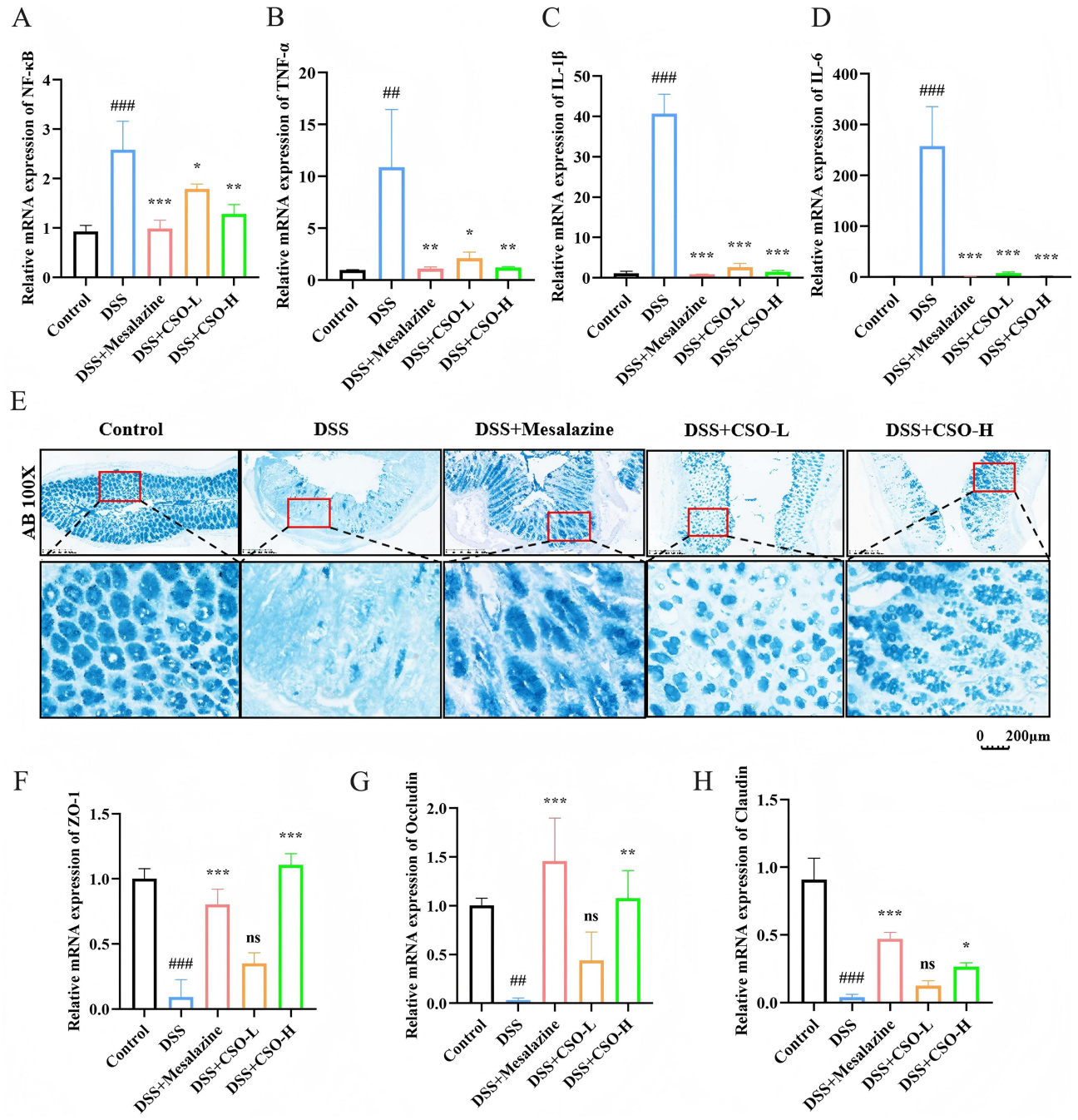

Figure 2 CSO reduced inflammatory biomarkers and alleviate DSS-induced intestinal barrier injury in DSS-induced mice. (**A**–**D**) Relative expression of inflammatory factors (TNF-α, NF-κB, IL-6, IL-1β) in colon tissues; (**E**) Alcian staining of cuprocytes in colon tissues (magnification, 100×; scale bar, 200 μm); (**F**–**H**) Relative expression of tight junction genes (ZO-1, Occludin, Claudin 1Ab) in colon tissues. n=3. The data were presented as the means ± SEM. $^{\#\#}P < 0.01$ and $^{\#\#\#}P < 0.001$, vs Control group; $^{*}P < 0.05$, $^{**}P < 0.01$, $^{***}P < 0.001$ vs DSS group.

Therefore, the Venn map displayed that 20 intersecting targets, which were considered to be potential targets of CSO against UC through ferroptosis pathway (Figure 3A).

DEGs Screening Results and Correlation Analysis of the Intersection Targets of "CSO-UC-Ferroptosis"

The above intersecting genes with significant differences were extracted from the test set GSE206285 after normalization, and 16 genes were found to be up-regulated in expression and 22 genes were down-regulated (Figure 3B). Correlation analysis demonstrated that the relationship between the significantly different genes, in which *PTGS2* had a

strong synergistic effect with *IL-6, KDM6B* and *ALOX5*, while *PPARA* had a strong antagonistic effect with *ENPP2, ALOX5* and *PTPN6* (Figure 3C).

GO and KEGG Enrichment Analysis of Intersection Targets of "CSO-UC-Ferroptosis"

The KEGG pathway and GO enrichment analyses of the "CSO-UC-Ferroptosis" intersection targets revealed that the biological process (BP) of the intersection target was focused on response to oxidative stress, cellular response to chemical stress. The molecular function (MF) focuses on chemical carcinogenesis-reactive oxygen species, choline metabolism in cancer, ErbB signaling pathway, HIF-1 signaling pathway, and IL-17 signaling pathway. The cellular component (CC) was enriched in the membrane raft and caveolae pathways (Figure 3D–F), and the top-ranked pathways may be the main mechanism of CSO in treating UC by regulating ferroptosis.

Screening Characteristic Intersection Targets of "CSO-UC-Ferroptosis" via Lasso and SVM Machine Learning

Lasso regression algorithm and SVM-RFE algorithm were utilized to identify seven genes as candidate characterization genes for UC, which included *MAPK8, AKR1C1, G6PD, KDM5C, KEAP1, PARP1, ABCC1* (Figure 4A–D). Taking the overlap of the genes obtained by the two different algorithms (Figure 4E), five characterized genes were obtained: *AKR1C1, G6PD, KDM5C, PARP1* and *ABCC1*. As shown in Figure 4F, the five characterized genes showed good diagnostic value in the test set. In the test group dataset, the AUC value of *PARP1* was 0.986, the AUC value of *ABCC1* was 0.985, and the AUC value of *G6PD* was 0.900, indicating that these 3 genes showed extremely excellent diagnostic value for CSO diagnosis of therapeutic UC through the ferroptosis pathway.

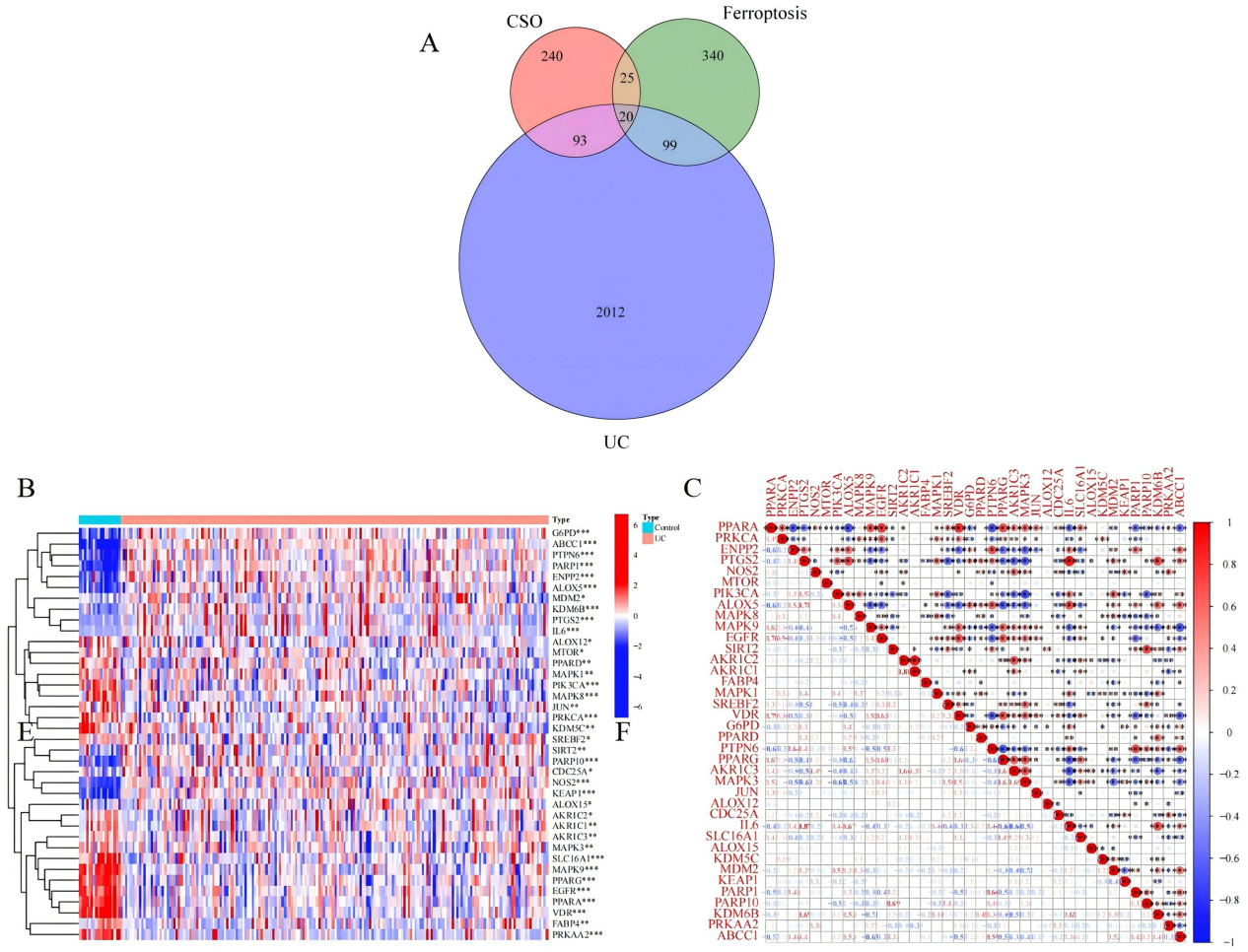

Figure 3 Continued.

https://doi.org/10.2147/JIR.S501745

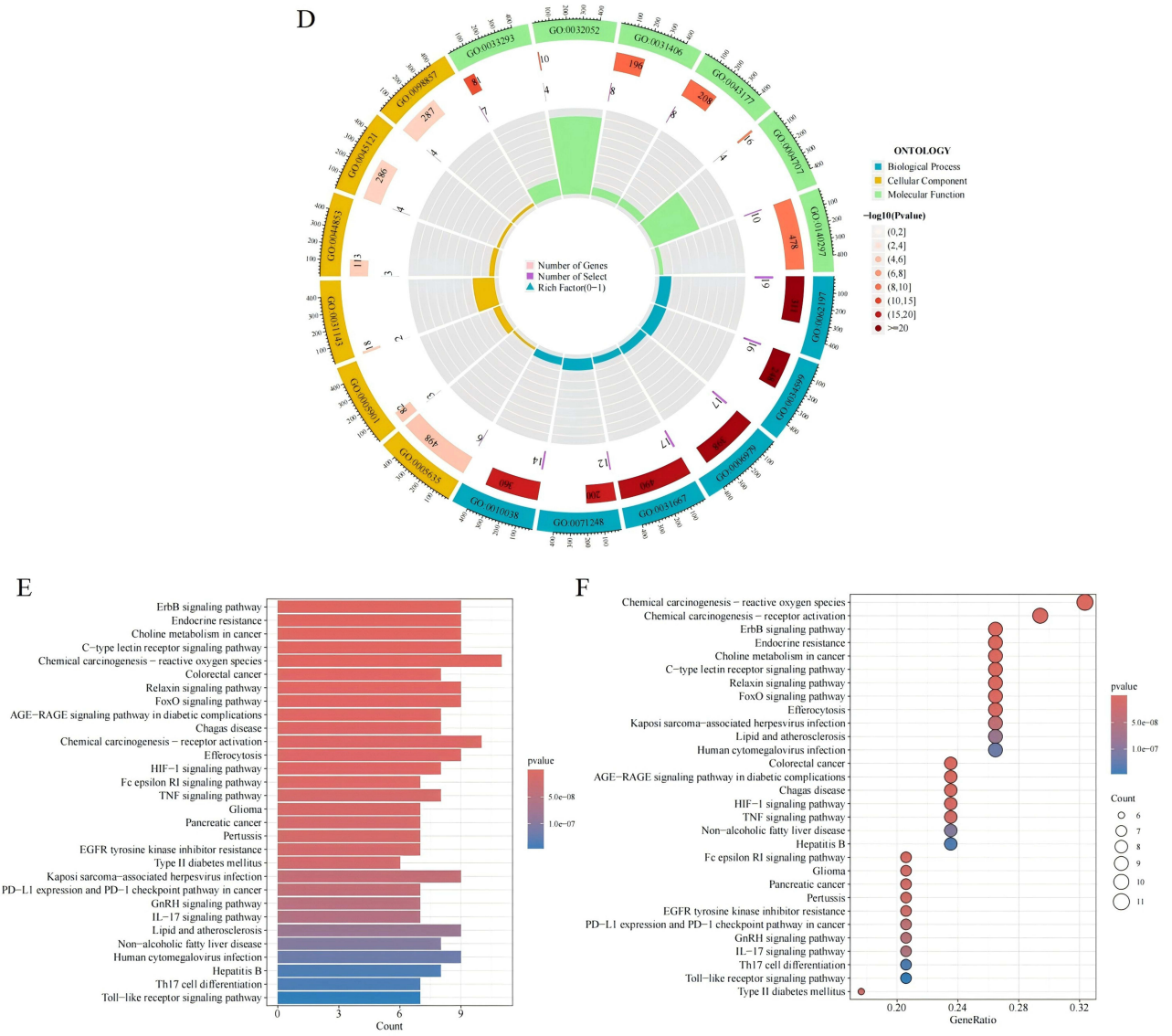

Figure 3 Screening of intersection targets and enrichment analysis of "CSO-UC-Ferroptosis". (**A**) Screening of candidate targets of "CSO-UC-Ferroptosis"; (**B**) Heat map of DEGs of the intersection targets of "CSO-UC-ferroptosis"; (**C**) DEGs correlation diagram of DEGs of the intersection targets of "CSO-UC-ferroptosis"; (**D–F**) GO and KEGG enrichment analysis of DEGs in intersection targets of "CSO-UC-Ferroptosis". *P < 0.05, **P < 0.01, ***P < 0.001.

GSEA Analysis

To further explore the regulation of different signaling pathways by the differential genes in the high- and low-expression groups, GSEA enrichment results showed that the top six pathways, chemokine-signaling pathway, cytokine–cytokine receptor interaction, focal adhesion, hematopoietic cellular regulatory signaling pathway, JAK-STAT signaling pathway and leishmaniasis infection, were actively expressed when *ABCC1* was expressed at low levels (Figure 5A). The results of *G6PD* and *PARP1* were similar to those of *ABCC1* (Figure 5B and C). *AKR1C1* was actively expressed in the focal adhesion, cytokine–cytokine receptor interaction and ECM receptor interaction pathways at low expression, while the cell cycle, DNA replication, and spliceosome pathways were suppressed (Figure 5D). Additionally, tumor, renal cell carcinoma, focal adhesion, and WNT signaling pathways were actively expressed at low *KDM5C* expression, whereas clip excision repair, and ribosome pathways were active at low expression (Figure 5E).

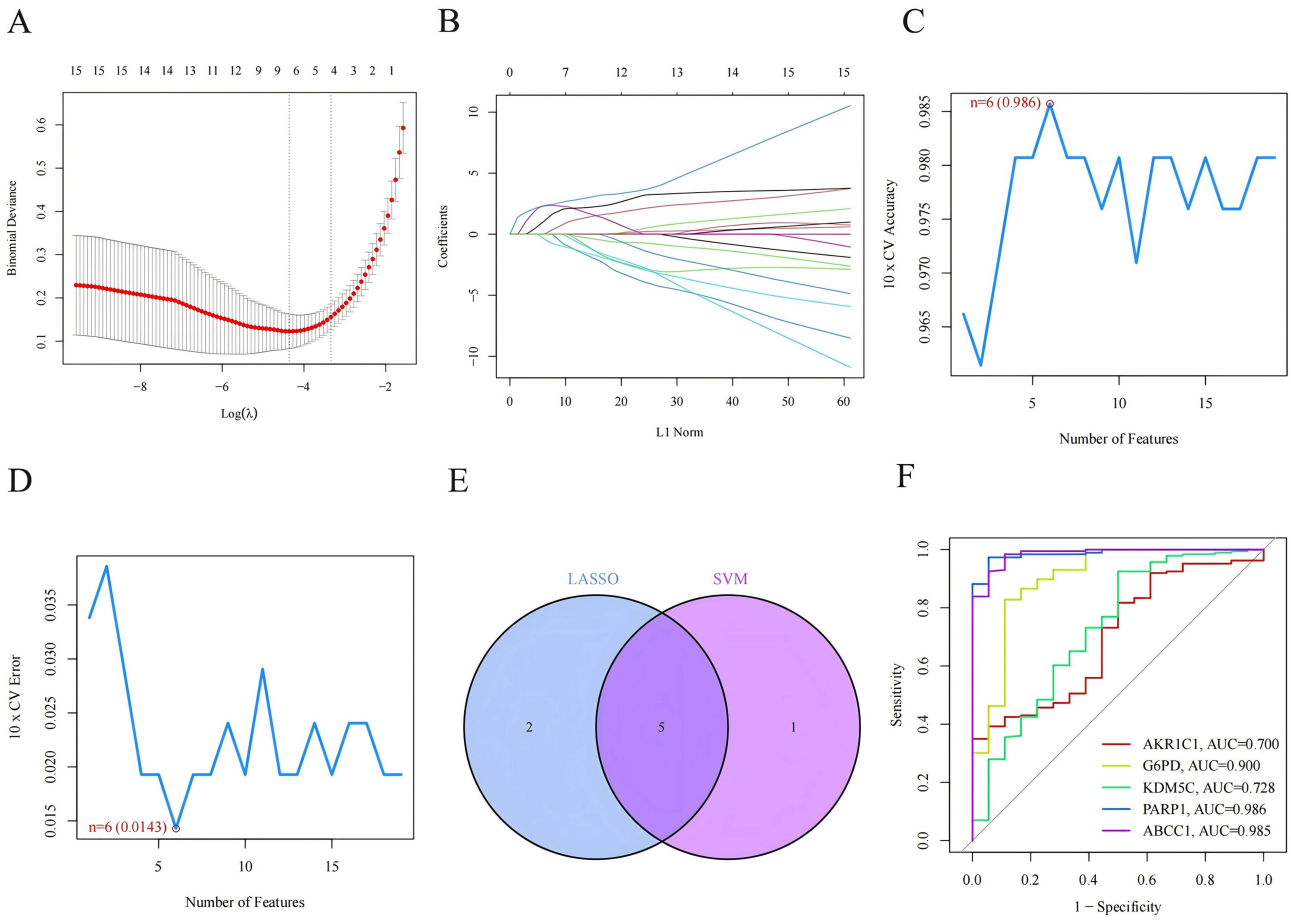

Figure 4 Lasso and SVM Machine Learning of Characteristic Intersection Targets of "CSO-UC-Ferroptosis". (**A**) LASSO Filter and draw the best parameters for vertical lines; (**B**) LASSO coefficient profiles of energy metabolism related genes; (**C**) SVM cross-validation accuracy graph; (**D**) SVM cross-validation error graph; (**E**) Intersection gene map; (**F**) ROC curves of characteristic genes of "CSO-UC-Ferroptosis".

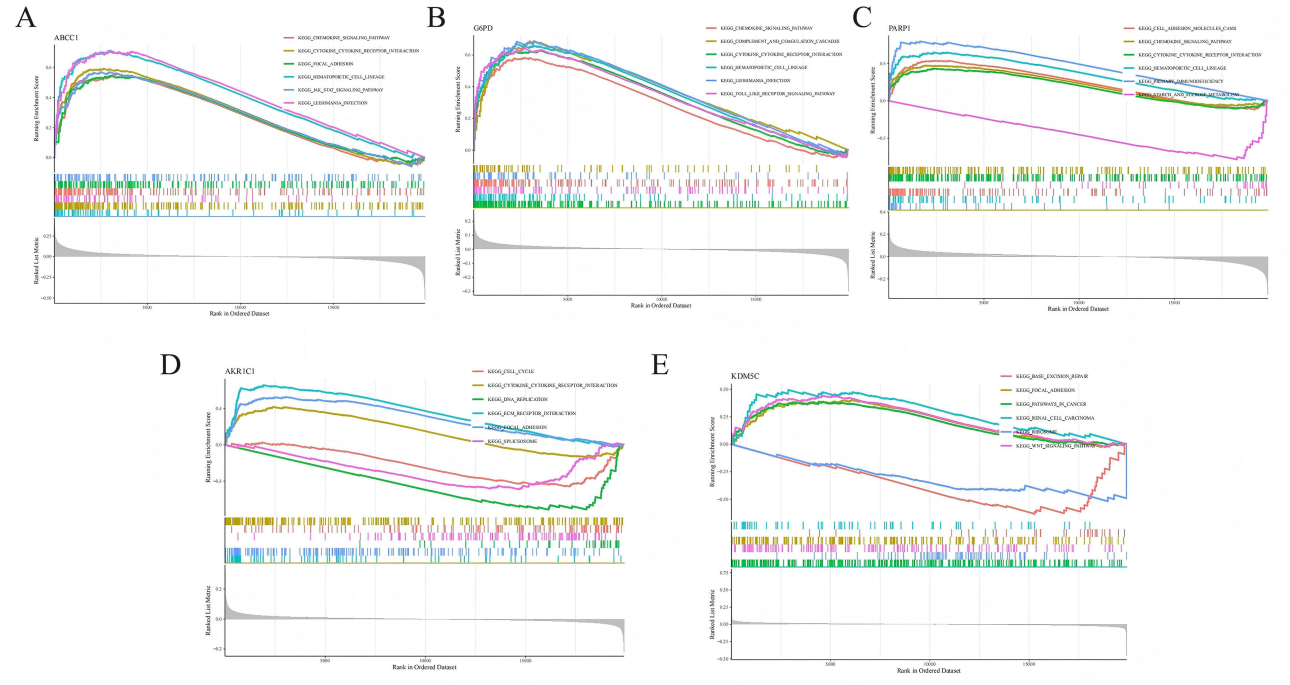

Figure 5 Continued.

https://doi.org/10.2147/JIR.S501745

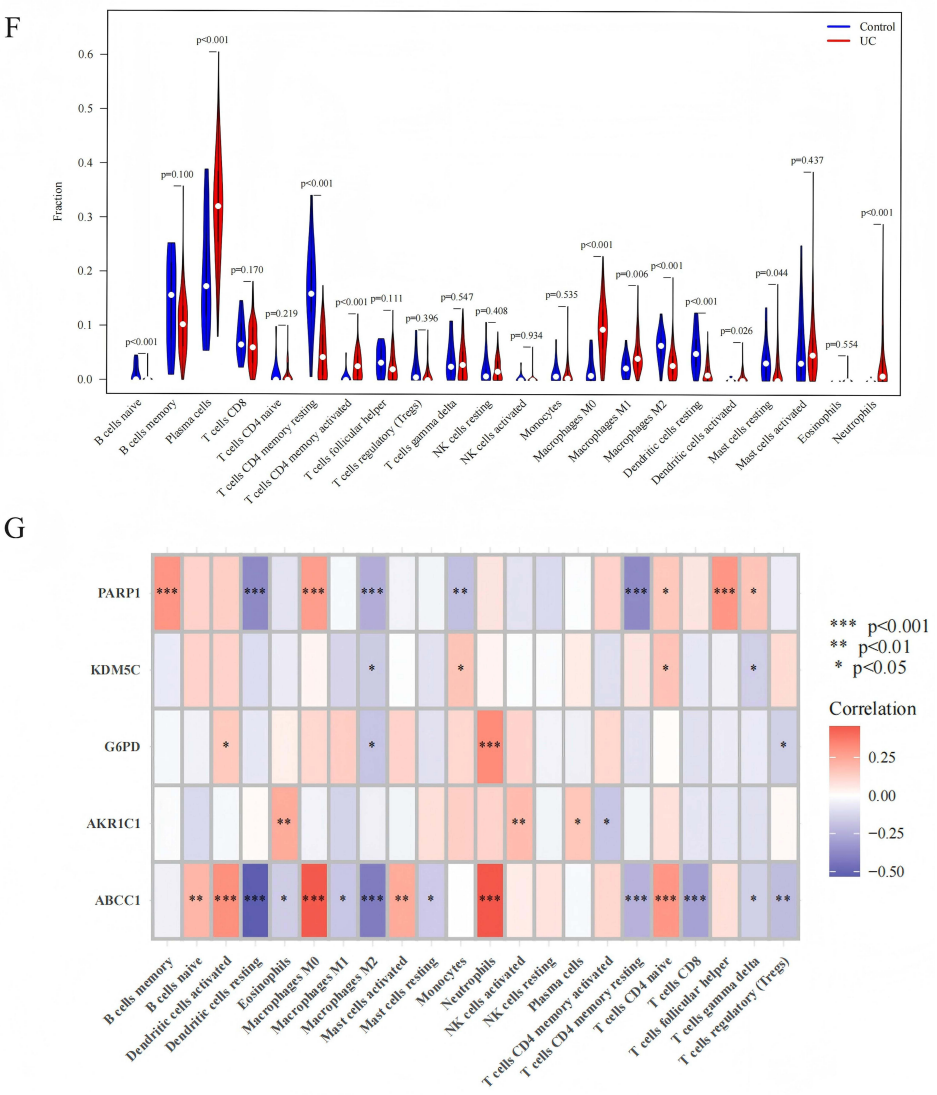

Figure 5 Explore the biological processes associated with FRGs. (**A**–**E**) GSEA analysis on *ABCC1, G6PD, PARP1, AKR1C1, KDM5C*. (**F**) Correlation between characteristic genes of "CSO-UC-Ferroptosis" and immune cells infiltration. (**G**) Heatmap of 22 immune cells correlations between characteristic genes in UC and healthy populations, the data were presented as the means ± SEM. **P* < 0.05, ***P* < 0.01 and ****P* < 0.001 vs Control group.

Immunoinfiltration Analysis

The results of immune infiltration analysis showed significant differences in immune cells between the UC group and the healthy control group, and the most significant differences in immune cell expression were observed in plasma cells, T cells CD4 memory resting, Macrophages M0 and Neutrophils, suggesting that the above cells are closely related to the pathogenesis of UC (Figure 5F). Further analysis of the immune infiltration of target FRGs in the above immune cells, the results indicated that *ABCC1* was positively correlated with M0 macrophages, neutrophils, and CD4+ T cells, and negatively correlated with resting dendritic cells and M2 macrophages. *G6PD* and *PARP1* had similar immune cell correlations as *ABCC1* (Figure 5G).

Validation of Characteristic Genes of "CSO-UC-Ferroptosis" and PPI Network Construction

To further verify whether the feature genes screened by machine learning in the validation set matched the test set, validation was performed by the validation set GSE87473. It was found that the expression of four genes, *AKR1C1, G6PD, PARP1* and *ABCC1*, were significantly different between the control group and the disease group (Figure 6A–D), while *KDM5C* was not significant (Figure 6E). The results of PPI network and topology analysis of potential targets of

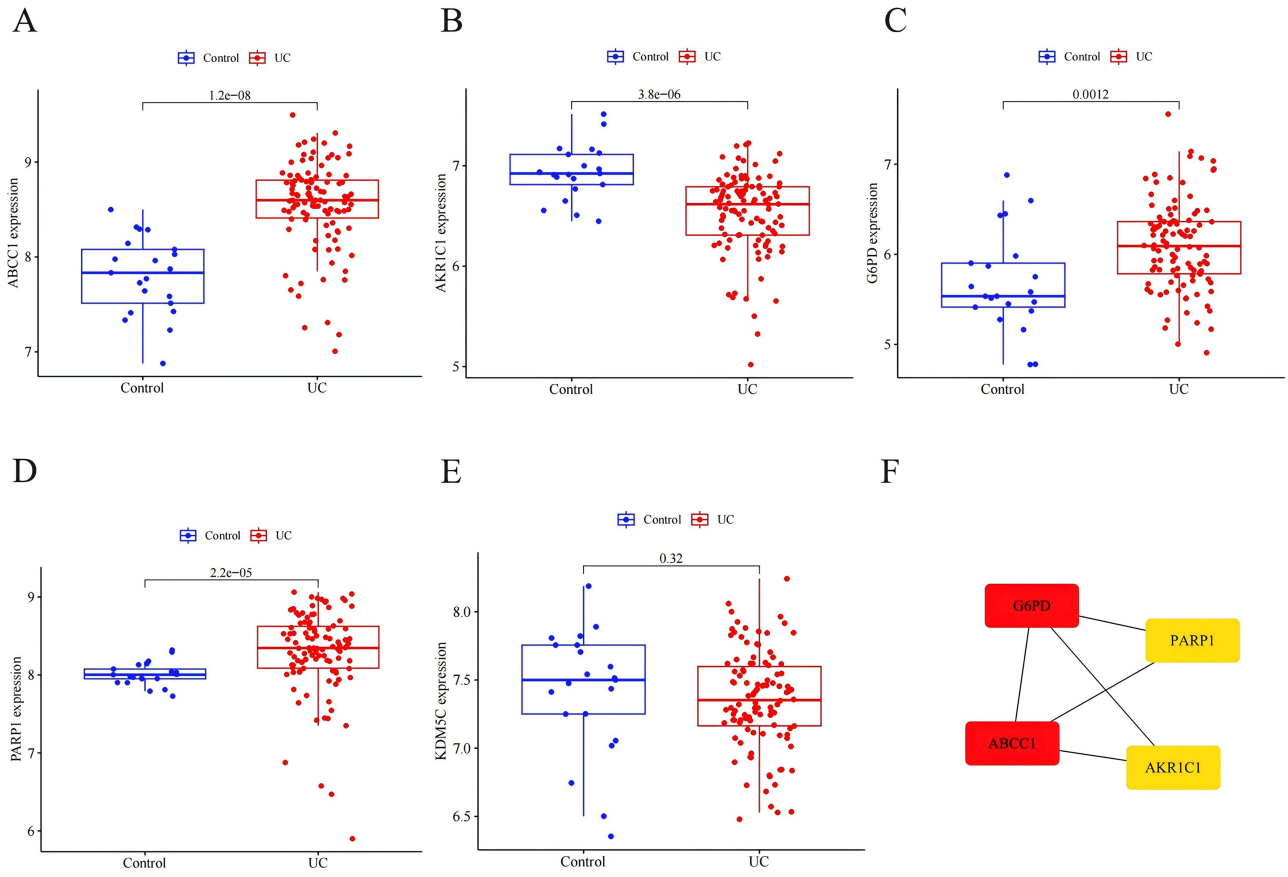

Figure 6 Validation and PPI Network Construction of characteristic genes of "CSO-UC-Ferroptosis". (**A**–**E**) Validation box diagram of characteristic genes of "CSO-UC-Ferroptosis"; (**F**) The core protein map of PPI network of "CSO-UC-Ferroptosis" targets.

action, the above CSO, UC, and ferroptosis intersecting genes, were uploaded to the STRING database, and a preliminary PPI network map was drawn to show the intersecting gene linkages in Cytoscape 3.9.1. Finally, following by the use of cytoHubba in accordance with the Degree sorting, we obtained *G6PD, ABCC1* as the core targets (Figure 6F).

Molecular Docking

The proteins expressed in the above core genes ABCC1, G6PD, PARP1 and AKR1C1 were molecularly docked with the active ingredients, stigmasterol and coixol, to further validate the binding ability of the CSO to the core targets. The docking results indicated that both ligands and receptors could spontaneously bind, and the binding energies (kcal/mol) of stigmasterol and coixol were −6.71 and −5.16 with MRP1 (ABCC1) (Figure 7A and B), - 5.59 and −5.08 with AKR1C1 (Figure 7C and D), -6.66 and -5.18 with G6PD (Figure 7E and F), and -8.43 and -5.62 with PARP1 (Figure 7G and H), respectively (Table 2). Residues of the ABCC1 target protein GLU-694, and the G6PD target proteins LYS-360 and GLY-242 had hydrogen bonding interactions with stigmasterol; while ABCC1 target proteins LEU-768, GLU-763, LYS-764 residues, G6PD target proteins TYR-507, THR-506 residues had hydrogen bonding interactions with coixol. These revealed that the monomer components in CSO have good binding activities with key gene target proteins.

CSO Alleviated UC Exacerbated by RSL-3

Ferroptosis plays an integral role in the physiology and pathophysiology of the intestine. Therefore, to further investigate the potential effect of CSO and the influence on ferroptosis in UC mice. An inhibitor (Fer-1) and an inducer (RSL-3) of ferroptosis have been used to explore the activity of CSO in treating UC through this pathway. Similarly, DSS is used as a modeling agent in animal models of UC. According to the results of the previous experiment, CSO at a dose of 50 mg/

https://doi.org/10.2147/JIR.S501745

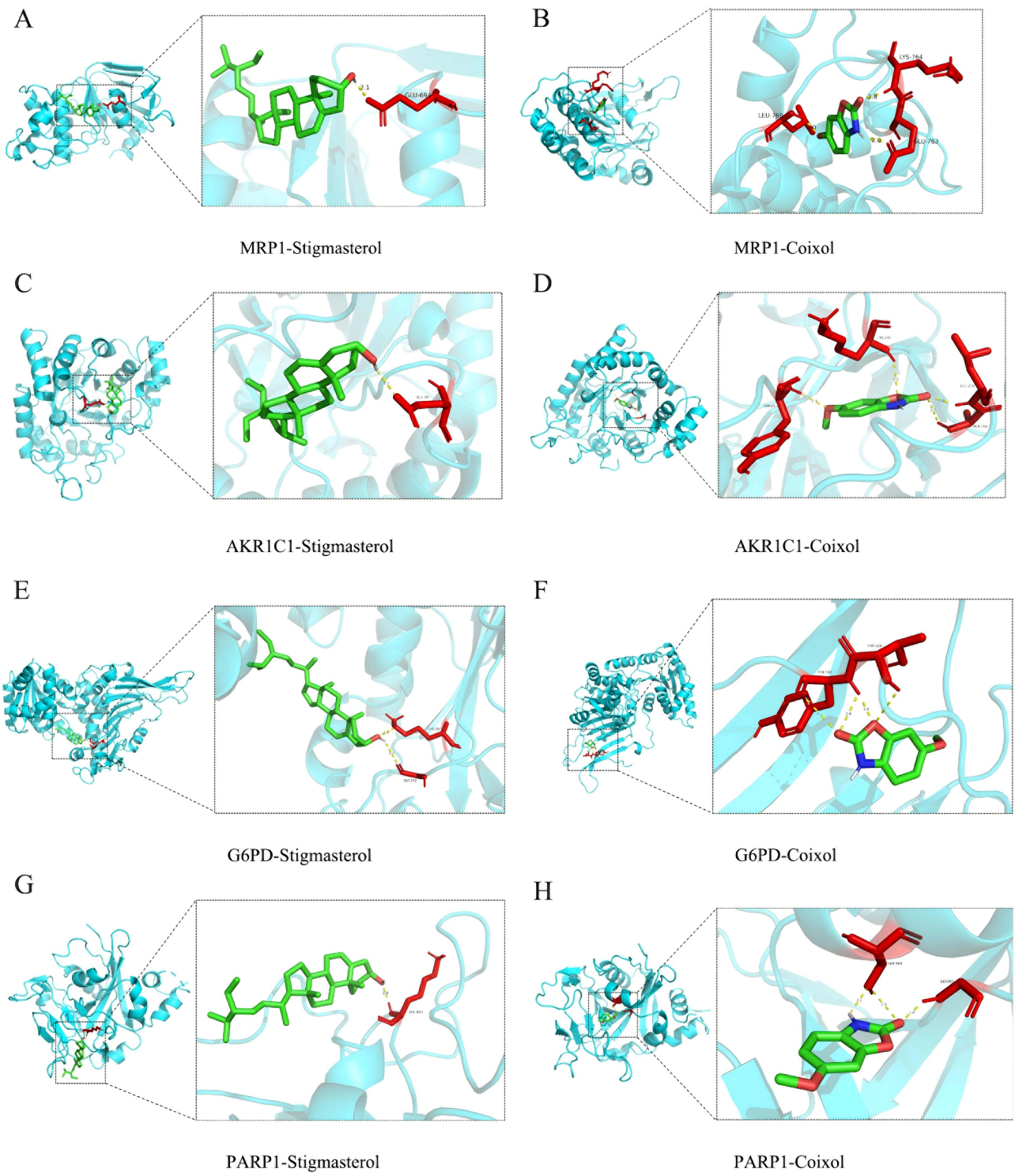

Figure 7 Molecular docking between FRGs and active ingredients of CSO. (**A–H**) Simulation of the docking between the potentially effective ingredients (Stigmasterol, Coixol) of CSO with *ABCC1*, *AKR1C1*, *G6PD and PARP1* protein.

kg was more potent, so this dose was chosen in verification experiment for the deeper experimental hypothesis (Figure 8A). At the end of the 11-day experiment, the same measurements of body weight change, colon length, and pathologic phenotype were performed.

Table 2 Molecular Docking Results of Core Targets

	Stigmasterol / (kcal/mol)	Coixol / (kcal/mol)
MRP1	−6.71	−5.16
G6PD	−6.66	−5.18
PARP1	−8.43	−5.62
AKR1C1	−5.59	−5.08

After 6 days of administration of 3% DSS drinking water, all model groups began to show a decreasing trend in body weight. Compared with the DSS group, a more pronounced trend of weight loss was observed in the DSS+RSL-3 group, while the sharp weight loss was well alleviated by the administration of both Fer-1 and CSO (Figure 8B). Colon length is one of the most important indicators of drug use for UC treatment. It can be seen that the mice in the DSS group and the DSS+RSL-3 group were lean, the colon was obviously shrunken and appeared to be red and swollen with ulcers, and the intestinal contents almost disappeared; whereas the situations of colon length shortening was not obvious in the DSS +Fer-1 group and the DSS+CSO group, and their mental status was better. In addition, even in the DSS+RSL-3+CSO group, which was injected intraperitoneally with the RSL-3 and then given CSO by gavage, the length of the colon was not significantly shortened, and the mice were in better condition (Figure 8C and D). In HE staining, it could be equally observed that the colons of mice in each model group were damaged to different degrees, especially in the DSS and DSS +RSL-3 groups, in which the crypts of the colonic tissues almost completely disappeared, and the DSS+RSL-3 group was more seriously damaged than the DSS group, with loose inter-tissue arrangement and severe inflammatory

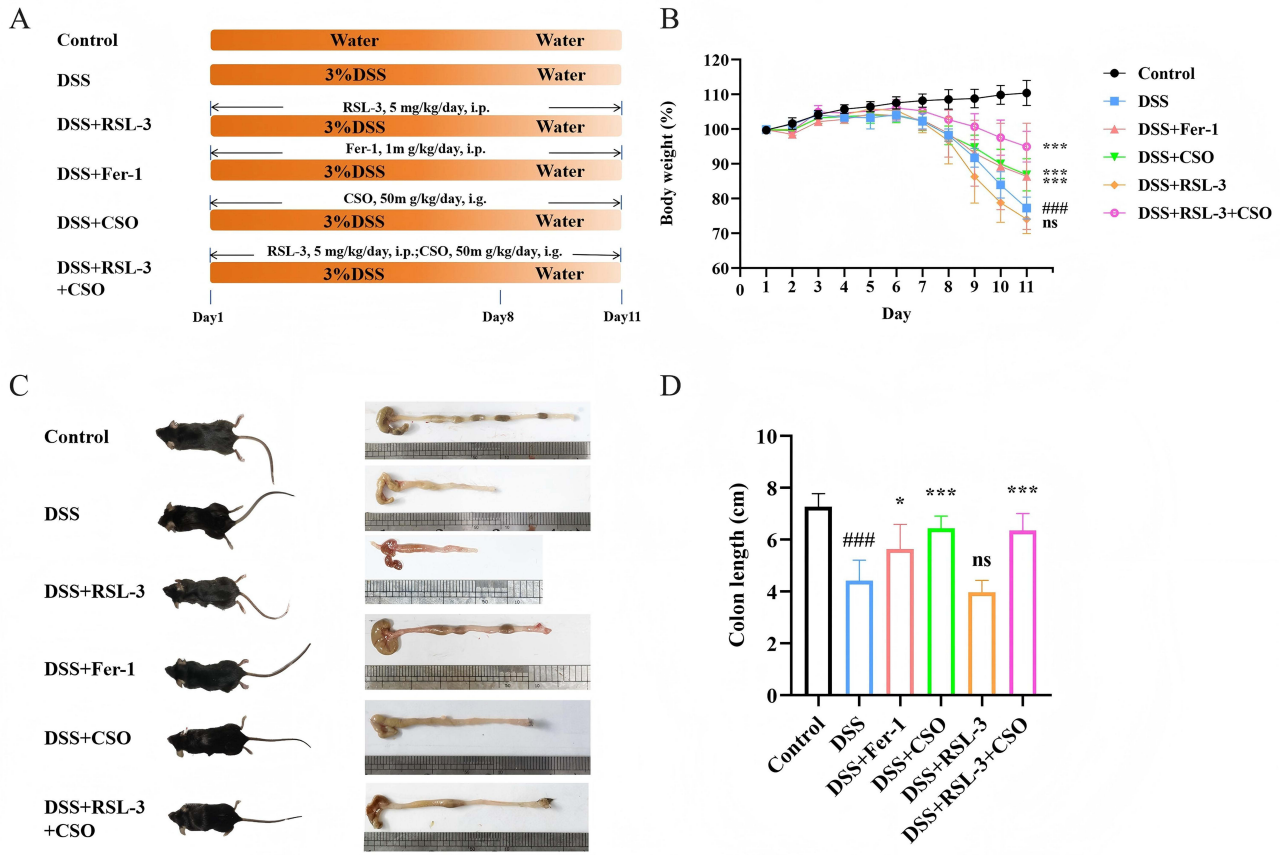

Figure 8 Continued.

https://doi.org/10.2147/JIR.S501745

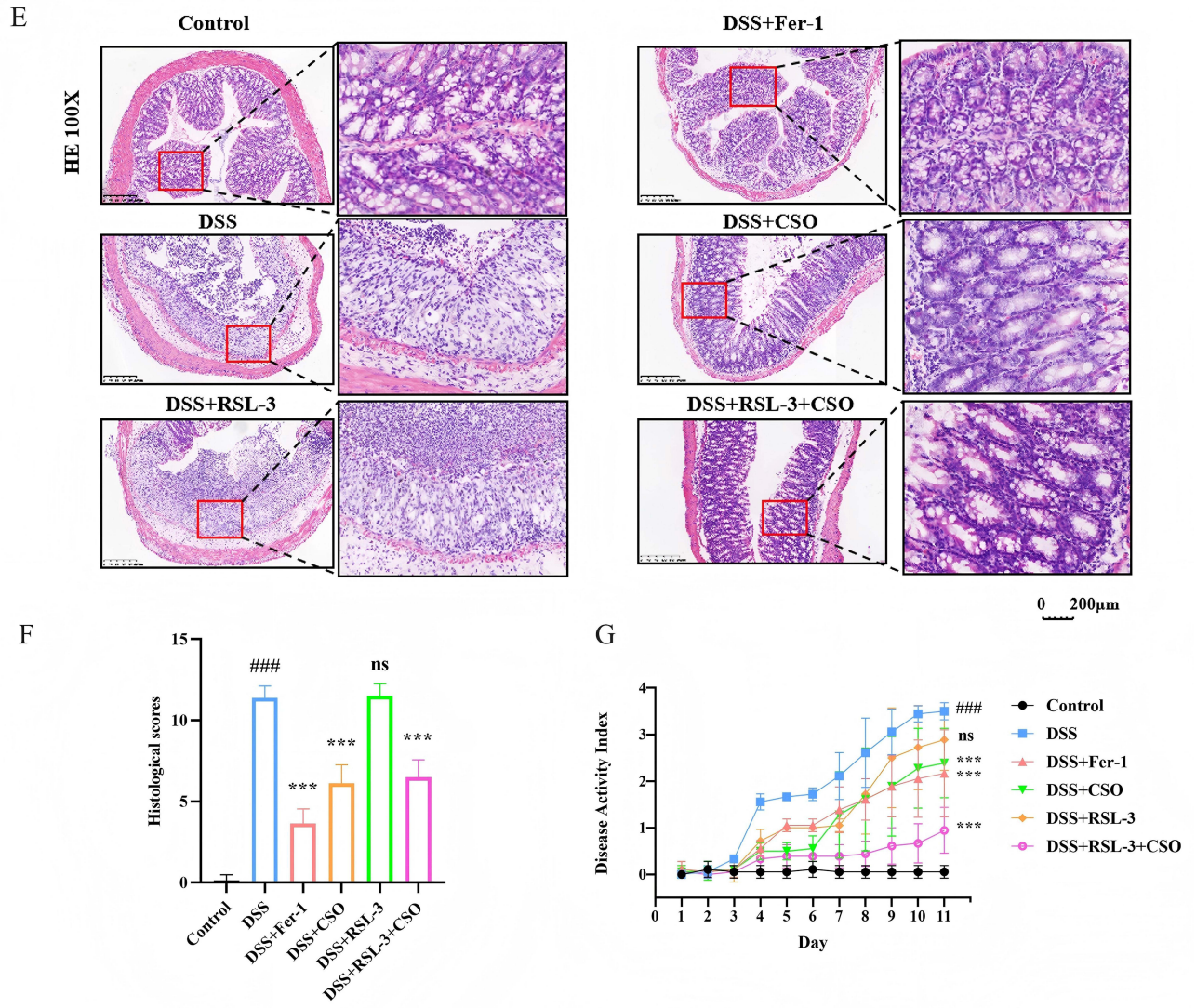

Figure 8 CSO Alleviated UC exacerbated by Ferroptosis inhibitors. (**A**) Experimental graph of the establishment of UC mice and the interventions of RSL-3, Fer-1, CSO, RSL-3+CSO, respectively; (**B**) Percentage change in body weight of all groups' mice; (**C**) Representative photographs of colons; (**D**) Comparison of colon length among the groups; (**E**) HE staining of colon tissues (magnification, 100×; scale bar, 200 μm); (**F**) Histopathological scoring of colon tissues; (**G**) Assessment of disease activity index. n=6. The data were presented as the means ± SEM. $^{###}P < 0.001$, vs Control group; $^{*}P < 0.05$ and $^{***}P < 0.001$ vs DSS group.

infiltration; the damage to the colonic tissues was significantly alleviated after the administration of Fer-1 and CSO (Figure 8E–F). Notably, the recovery of colon tissues and disease activity index appeared to be more effective in the administration group given RSL-3, suggesting that CSO may have a protective effect on UC through the ferroptosis pathway (Figure 8G).

CSO Alleviated Intestinal Barrier Injury in RSL-3-Stimulated UC Mice

In order to further investigate the mechanism of CSO against UC after the administration of ferroptosis inducers, we firstly used AB staining to observe the number and distribution of goblet cells in the colonic tissues of mice in each group. The results showed a similar damage with the HE staining, which the damage of cup cells in the colon tissue of mice after DSS modeling was severe to the point of disappearance, and the same phenomenon of crypts and cuprocypes disappeared significantly after the administration of RSL-3, whereas the inter-tissue gaps were larger and loosely arranged, which indicated that the colon damage in this group of mice might be more severe; after the administration of either Fer-1 or CSO, the cellular organization morphology had improved to different degrees, while the tissue structure

of the DSS+RSL-3+CSO group appeared to be more complete compared with the CSO group (Figure 9A). In addition, the exploration of intercellular connections in colonic tissues was performed by transmission electron microscopy (TEM), and the intercellular connections in the control group were tight and clear; the intercellular connections in all groups showed clefts or damage after DSS modeling. Compared with the DSS group, the intercellular junction damage was reduced or even restored in the DSS+Fer-1 and DSS+CSO groups, whereas the tight junctions in the DSS+RSL-3

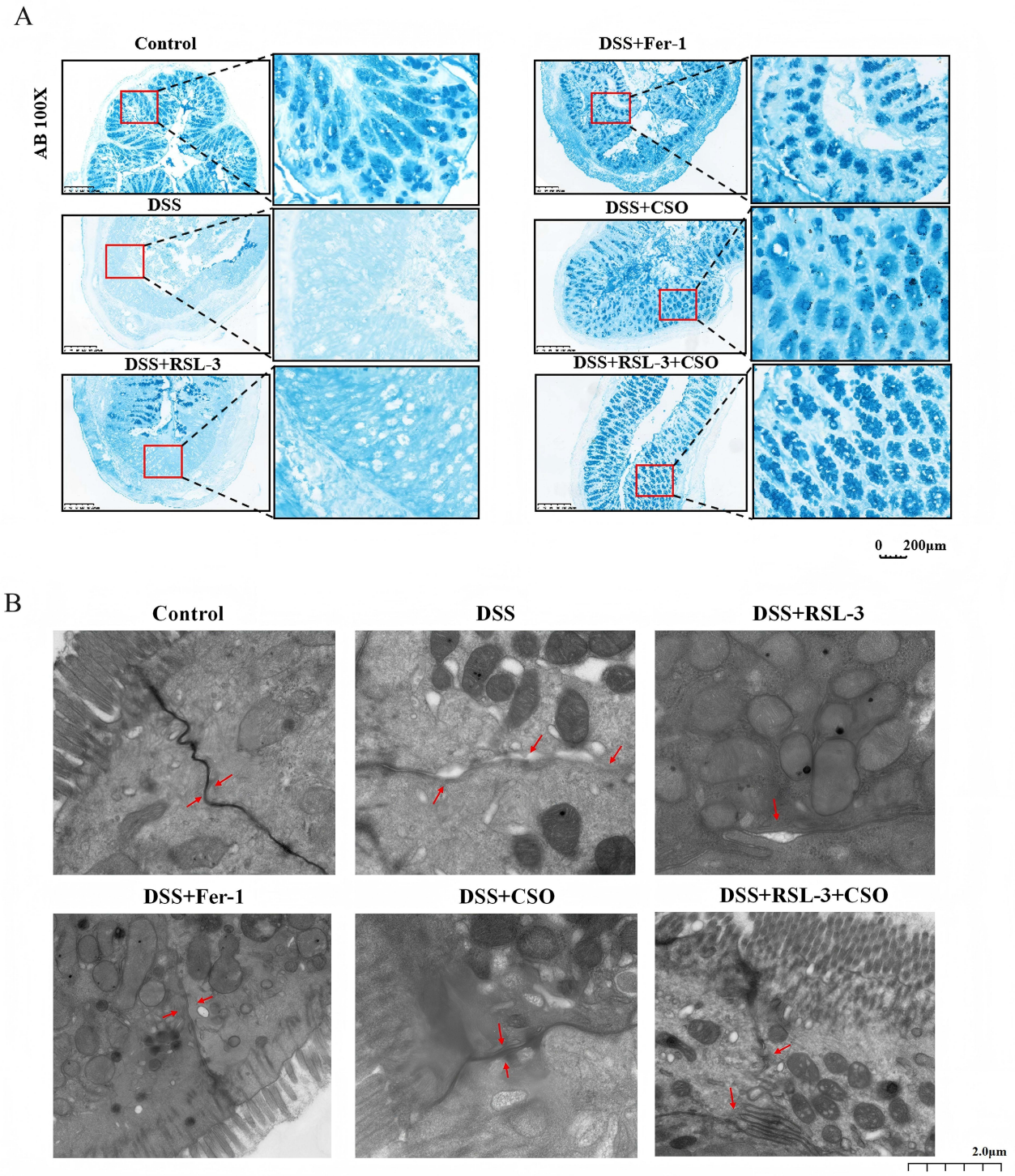

Figure 9 Continued.

https://doi.org/10.2147/JIR.S501745

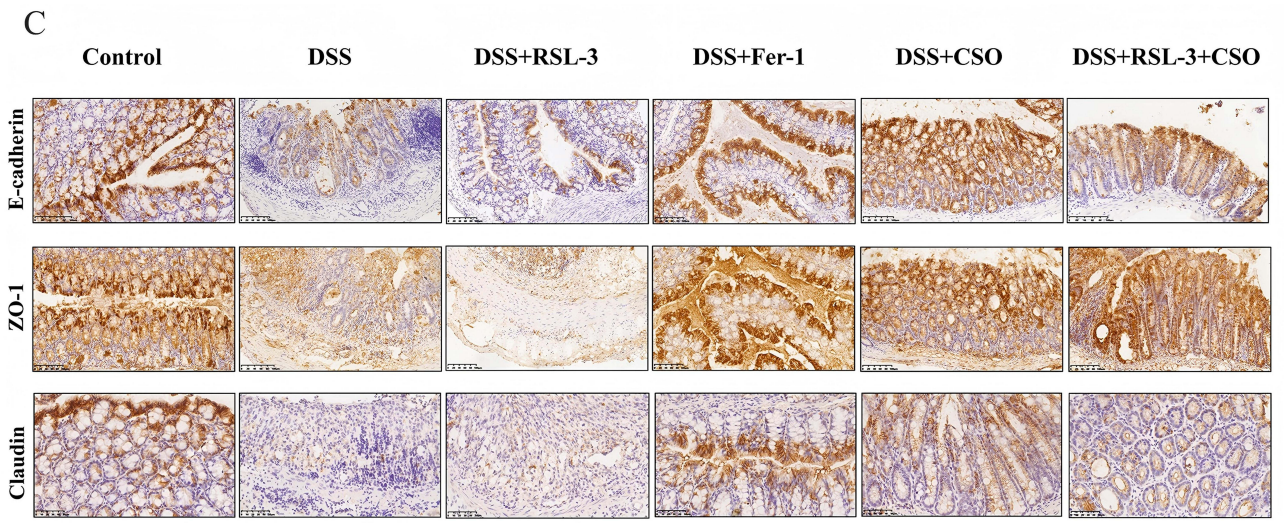

Figure 9 CSO Alleviated Intestinal Barrier Injury in Ferroptosis-inhibited UC mice. (**A**) Alcian staining of cuprocytes in colon tissues (magnification, 100×; scale bar, 200 μm); (**B**) Observation of intercellular connections between colon tissues in each group under transmission electron microscope(TEM), the red arrows refer to the state of intestinal epithelial intercellular junctions, which can be seen as tight intercellular junctions in the control group, disrupted intercellular junctions with breaks and clefts in the DSS and DSS+RSL-3 groups, and protected from disruption of intercellular junctions in the DSS+Fer-1, DSS+CSO and DSS+RSL-3+CSO groups (magnification, 10000×; scale bar, 2 μm). (**C**) Expression of tight junction protein (E-cadherin, ZO-1 and Claudin) in colonic tissues of different groups by immunohistochemical assay.

+CSO group were damaged but the junctional filaments appeared to be increased (Figure 9B). As mentioned previously, TJ proteins are important measures of the integrity of intestinal tissue barrier protection. Therefore, we further examined the expression of each TJ protein among colonic tissues by immunohistochemistry. The results showed that the expression of TJ proteins was significantly decreased after DSS modeling, especially E-cadherin, ZO-1 and Claudin, and the protein expression was clearly elevated and more enriched in the location of intestinal epithelial cells after the administration of Fer-1 and CSO, which suggests that CSO treatment of UC may be related to its promotion of intestinal barrier repair (Figure 9C).

Regulation of CSO on Ferroptosis in UC Mice May Related to Mitophagy

As a non-regulatory mode of cell death induced by oxidative damage, ferroptosis is closely associated with ROS accumulation and inflammatory response, which is also believed to be an important cause of persistent colonic injury leading to the pathogenesis of UC. In the present experiment, we tested the relevant index components by the kit and observed that after the administration of DSS modeling, the total iron ions and MDA concentrations in the colonic tissues of mice increased significantly (Figure 10A and B), and the SOD content decreased significantly (Figure 10C), which was not statistically different from that of the DSS+RSL-3 group given ferroptosis inducer, indicating that there was an excess of OS and increased injury. After administration of Fer-1 and CSO, the total iron ion and MDA concentrations decreased to normal values, SOD content recovered.

Mitochondria play a central role in cellular iron metabolism, and high concentrations of iron make mitochondria an ideal site for inducing ferroptosis. Therefore, TEM was also used to observe the changes in the morphology of mitochondria in the cells of the colon tissue to investigate the severity of ferroptosis in the colon of each group of mice. In the normal group, the inner and outer mitochondrial membranes and cristae were clearly visible; whereas the mitochondria in the intestinal cells of mice in the various modeling groups were shrunken, the outer membranes were ruptured, and the cristae of the mitochondria were enlarged, which was alleviated and mitochondrial morphology was restored after the administration of Fer-1 and CSO (Figure 10D). Notably, an increase in the number of mitochondria was observed in the TEM images of the DSS+RSL-3+CSO group, and a significant increase in autophagic vesicles appeared in the mitochondria, suggesting that CSO may alleviate excessive ferroptosis by activating mitophagy.

Then, to further verify whether the core targets predicted by network pharmacology and bioinformatics were effective for the prevention and treatment of UC. Immunohistochemistry was used to detect the CSO's effects via which pathway

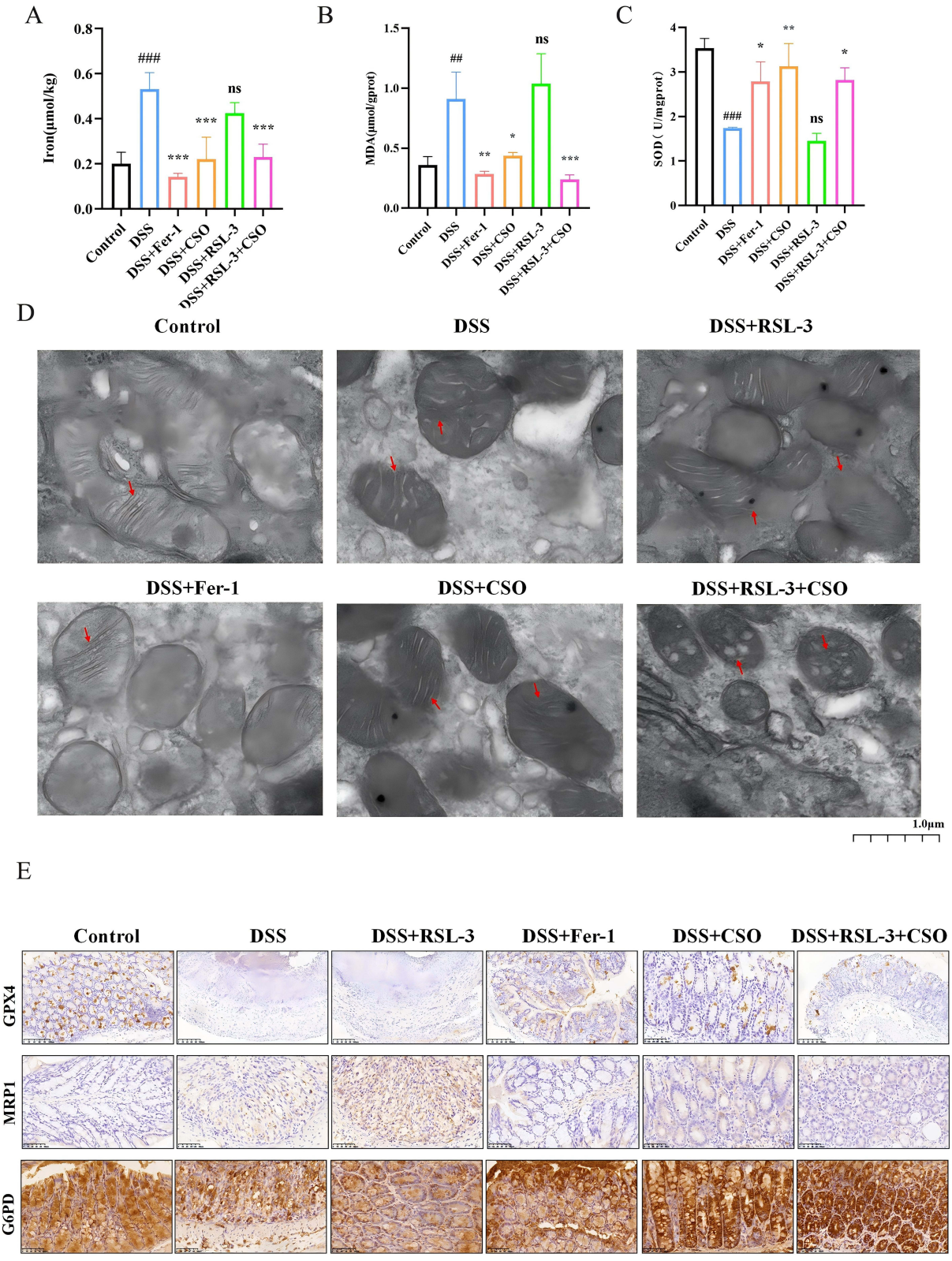

Figure 10 Regulation of CSO on ferroptosis in UC mice may related to mitophagy. (**A**–**C**) Iron, MDA, SOD content of colon tissue in mice, n=3. (**D**) Observation of mitochondrial morphology of colon tissues in each group under TEM, the red arrows refer to changes in mitochondrial membrane and mitochondrial cristae morphology (magnification, 10000×; scale bar, 1 μm). (**E**) Expression of ferroptosis-related protein (GPX4, MRP1, G6PD) in colonic tissues of different groups by immunohistochemical assay. The data were presented as the means ± SEM. $^{\#\#}P < 0.01$ and $^{\#\#\#}P < 0.001$, vs Control group; $^{*}P < 0.05$, $^{**}P < 0.01$, $^{***}P < 0.001$ vs DSS group.

https://doi.org/10.2147/JIR.S501745

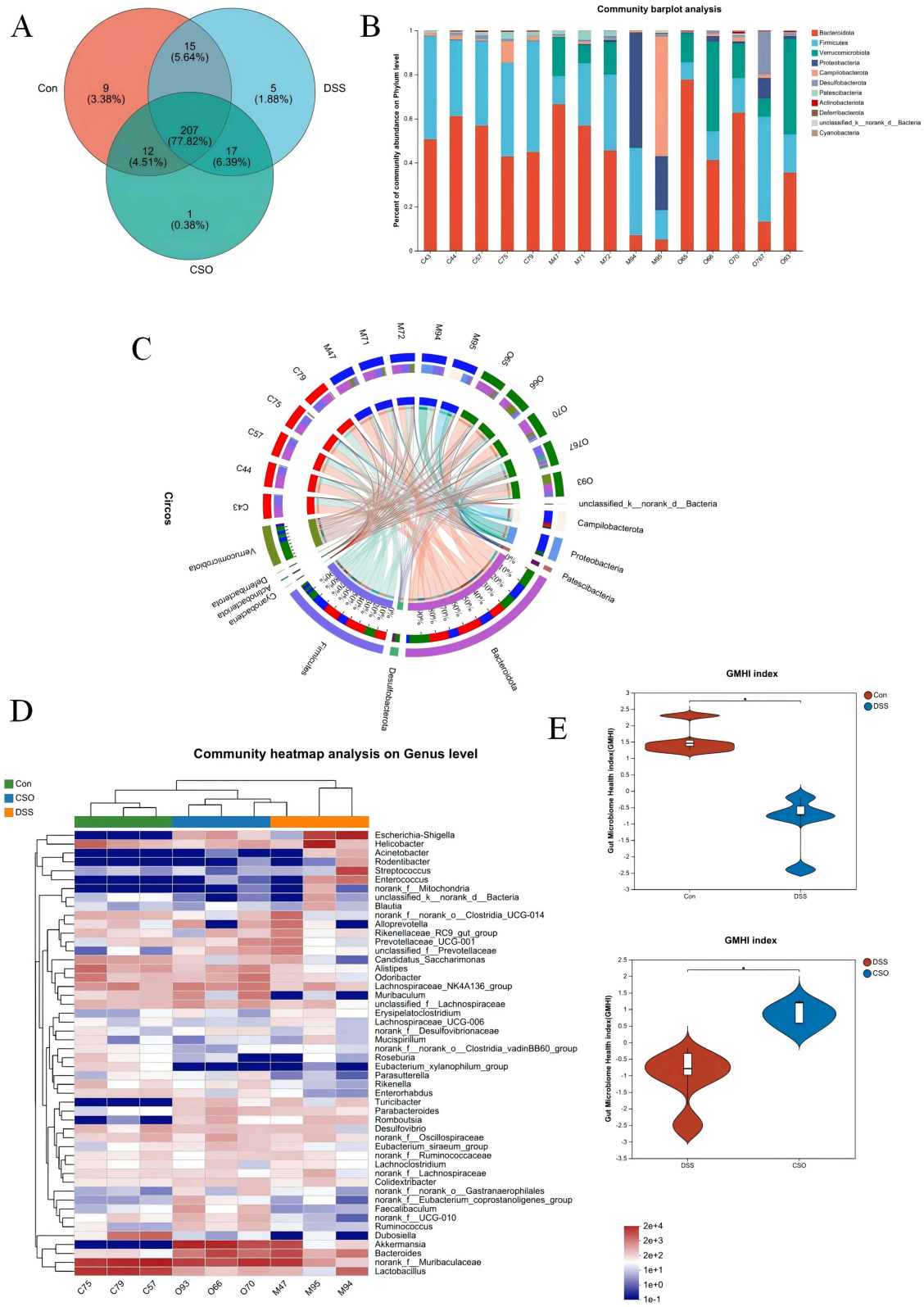

Figure 11 CSO regulates the structure of intestinal flora in DSS-induced UC mice. (**A**) Venn diagram of OTU among control, DSS and CSO groups. (**B**) Community barplot analysis. (**C**) Circos Sample-Species Relationship Map. (**D**) Community heatmap analysis in genus level. (**E**) Gut microbiome health analysis between control and DSS groups, DSS and CSO groups. n=3-6. *P < 0.05 vs DSS group.

for the treatment of DSS-induced UC mice. As predicted, CSO treatment significantly restored the increase in GPX4 and MRP1 and decrease in G6PD content in colonic tissues due to the exacerbation of ferroptosis in UC (Figure 10E).

Effects of CSO Administration on Gut Microbiota

In recent years, dysbiosis of the intestinal microbiota has been recognized as a risk factor for the progression of UC.[37] To explore changes in gut microbiota following CSO administration, colon content samples were collected for DNA extraction and sequencing from the control, DSS model and CSO groups. Notably, the variations within the CSO group are significant than other groups (Figure 11A). In terms of community composition, it was evident that the DSS group differed significantly from the control and CSO groups at the phylum level, as evidenced by an increase in the proportions of the *Proteobacteria* and *Campilobacterota*, while after CSO administration, the abundance of *Verrucomicrobiota*, which are associated with intestinal anti-inflammatory effects, notably enhanced compared to other bacteria (Figure 11B). Similarly, the Circos Sample-Species Relationship Map presents that the species composition of the control group was dominated by *Bacteroidota* and *Firmicutes*. After DSS modeling, there was a significant decrease in the abundance of the above two types of bacteria, which was replaced by an increase in the abundance of *Campilobacterota* and *Proteobacteria*, which are associated with enteritis pathogenesis. In contrast, in the CSO group, the abundance of *Campilobacterota* and *Proteobacteria* decreased significantly and *Bacteroidota* and *Firmicutes* converged to the level of the control group (Figure 11C).

Routine Alpha-diversity and Beta-diversity analyses indicated that CSO restored the changes in gut microbial abundances and diversity due to DSS modeling (Figure S1). Then, we further performed species difference analysis, and at the genus level, a significant decrease in *Dubosiella, Enterorhabdus* and *Rikenella* after DSS modeling, which were all restored after CSO administration (Figure 11D). In addition, the health status of intestine was assessed by gut microbiome health analysis (GMHI), a method for obsessing health status based on species-level taxonomic characterization of gut microbiome samples, which is often considered a marker of gut health and ecological dysbiosis. We found that the GMHI index was significantly elevated after DSS modeling, while surprisingly decreased after administration of CSO, suggesting that CSO has a role in the regulation of healthy gut microbes, which is also consistent with the previous results (Figure 11E).

Discussion

As a lifelong intestinal disease caused by excessive inflammatory, UC has always been susceptible to recurrence due to its onset and the limitations of clinical medication.[38] Therefore, finding suitable therapeutic targets and exploring effective drugs to prevent and treat UC has become an urgent problem. TCM have accumulated rich experience in the treatment of UC-like symptoms, containing unique advantages with repairing the intestinal mucosal barrier, regulating immunity and intestinal flora to alleviate UC.[39,40] To a certain extent, it can improve the overall clinical effectiveness rate, reduce the level of serum inflammatory factor and the score of intestinal mucosal pathologic examination of the patients.

Coix lacryma-jobi is derived from the TCM formula, Yiyi Fuzi Baijiang San (YFBS), which is from Zhang Zhongjing's "The Essentials of the Golden Chamber" of the Eastern Han Dynasty, and was first used in the treatment of intestinal carbuncle, and now it is a classic formula for the treatment of UC and inflammation-associated colorectal cancer (CRC) in the clinic.[41,42] Among them, *Coix lacryma-jobi*, as the most important drug in this formula, its extracts, especially CSO, have been widely used in the treatment of breast cancer, primary non-small cell lung cancer and primary liver cancer.[43,44] As a kind of TCM used for both food and medicine, the application of CSO is safe. The effective human dose for the preparation of CSO, kanglaite injection, is 200 mL/day. We found that the dose of CSO in animal experiments should be less than 50 mg/kg through preliminary literature research and pre-experimentation.[45,46] Therefore, the selectable dose was chosen 50 mg/kg as the high dose and 12.5 mg/kg as the low dose in this study, to test our hypothesis about the use of CSO for anti-UC.

As mentioned earlier, UC is an intestinal barrier disease, initially triggered by functional damage to the intestinal epithelium, whose cascade subsequently leads to chronicity of the disease. Our study firstly found that CSO has a protective effect on the intestinal barrier and that disease progression and colonic tissue damage were significantly

attenuated in UC mice after administration of CSO. In addition, numerous studies have found that ferroptosis is involved in UC disease progression. Several recent studies have shown that in the DSS-induced UC model, the application of ferroptosis inhibitors (Ferrostatin-1 and Liproxstatin-1) resulted in a significant increase in the body mass and colon length of UC mice, and significant alterations in ferroptosis-related markers, suggesting that ferroptosis is closely associated with UC.[47,48] Therefore, in combination with the results of the pre-test, we hypothesized that the anti-UC effect of CSO was related to ferroptosis.

GPX4 is the fourth member of the selenium-containing GPX family, which can inhibit the occurrence of ferroptosis in cells by reducing lipid peroxidation. The down-regulation of GPX4 is thought to be a key feature of ferroptosis. SLC7A11 is an important component of the cystine glutamate transporter receptor (system Xc-) of the body antioxidant system. In normal conditions, system Xc- can transport extracellular cystine to the cell and participate in the synthesis of glutathione, which helps the body to scavenge excess ROS and protects cells from OS damage; whereas blocking system Xc- leads to the blockage of GSH synthesis, which impairs cellular antioxidant capacity, and then leads to the generation of ferroptosis.[49] To verify the effect of GPX4 in UC, we intraperitoneally injected mice with RSL-3, which directly binds to the GPX4 protein receptor, to induce the development of ferroptosis in vivo. From the HE staining and AB staining of pathological sections, we could see that in RSL-3 group, the number of cuprocytes in the colonic tissues was less or even disappeared, and the damage of crypt structure was more serious compared with that of the DSS model group, whereas the pathological damage was alleviated to a greater extent in the Fer-1 group given the ferroptosis inhibitor. The alleviation of colonic tissue barrier damage after administration of CSO was similar to that in the Fer-1 group, and the effect remained significant even after the addition of RSL-3. G6PD is an enzyme present in human erythrocytes to assist in the metabolism of glucose, and during metabolism NAPDH is produced. NAPDH can be used to maintain the reduced state of GSH, who plays an important role in the maintenance of the content of reduced GSH in cells. When excessive ferroptosis occurs in the organism, GSH synthesis is blocked and its content decreases significantly, as does the content of G6PD. Some studies have found that G6PD can promote the proliferation, migration and invasion of HCC cells and inhibit ferroptosis; after knockdown of G6PD, it can reduce the volume and weight of tumors in vivo, which suggests that G6PD may be used as a potential target for anti-tumor and inhibition of ferroptosis therapies, and this is also in line with the results of this study.[50]

Furthermore, the role of intestinal flora alterations in the progression of ulcerative colitis (UC) has been extensively researched and recognized as a significant factor. The intestinal flora of UC patients undergoes notable changes, with a reduction in beneficial bacteria such as *Bifidobacterium* and *Lactobacillus*, and an increase in harmful bacteria like enterotoxigenic. This alteration directly impacts the metabolic products of the intestinal flora, such as the decrease in short-chain fatty acids (SCFAs) like butyrate, which play a protective role in intestinal metabolism by regulating the proliferation and development of intestinal epithelial cells and maintaining the integrity of the intestinal epithelial barrier.[51] When these protective factors decrease, the intestine becomes more susceptible to inflammatory attacks, leading to the occurrence and progression of UC. Similarly, our study found that the abundance of harmful bacteria in UC mice, like *Proteobacteria* and *Campilobacterota*, were markedly higher than control mice, which were related to induce enteritis and diarrhea. Luckily, the percentage of harmful bacteria were declined after CSO administration, while the proportion of beneficial bacteria was restored. This trend also demonstrated the same in GMHI index. In summary, oxidative stress was significantly increased in mice after administration of RSL-3, which was accompanied by increased ferroptosis as well as intestinal barrier damage, in addition to dysbiosis of the intestinal flora, which was also ameliorated by the intervention of CSO. Thus, the effect of CSO in the treatment of UC is likely to be related to the recovery of intestinal barrier integrity combined effects of reduced oxidative stress (via ferroptosis inhibition) and restored microbial homeostasis. These findings suggest that CSO could serve as a cost-effective adjunct therapy for UC, pending validation in clinical settings.

However, there are still some limitations in this study. Firstly, the bioinformatics parts of this study were mainly based on public databases, to explore the targets related to drug action, and the accuracy and timeliness of the database data still need to be examined. The main active ingredients selected in this study are based on the pharmacopoeia and previous studies to screen the representatives, which do not fully represent all the components of the CSO action and be optimized for enhanced efficacy. While the DSS model is a well-established UC model, it represents acute colitis, the possibility that for drug studies chronic UC models may be able to better simulate human pathogenesis, a limitation that will be

considered for in-depth validation by adopting a complementary chronic model in future studies. Although our study provides possible drug alternative possibilities for the treatment of UC. However, due to safety concerns, this paper lacks sufficient sample for relevant preclinical findings and clinical application considerations, and further validation is needed.

Conclusion

In conclusion, this study found that the anti-UC effect of CSO is likely to be related to recovery of intestinal barrier integrity via ferroptosis inhibition and restored microbial homeostasis, but also need for further experimental validation of bioinformatic predictions and molecular docking results. Our study not only revealed the possibility of inhibiting ferroptosis to protect the intestinal barrier for the treatment of UC but also emphasise the potential for CSO to be developed as a clinical treatment into human studies.

Data Sharing Statement

The data used to support the findings of this study is confidential.

Acknowledgments

All authors thank all the research participants contributing to the GEO resource for providing high-quality data for analysis. We would also like to express our sincere gratitude to Mr. Chao-Hua Luo for his magnanimous financial contribution to our research, as well as for his valuable assistance pertaining to the survey research and methodology.

Funding

This research was supported by the, Natural Science Foundation of Guangdong Province (Grant No.2023A1515011060), Scientific Research Project of Guangdong Provincial Bureau of Traditional Chinese Medicine (Grant No.20251247).

Disclosure

The authors declare that they have no conflicts of interest in this work.

References

1. Dai C, Huang YH, Jiang M. Combination therapy in inflammatory bowel disease: current evidence and perspectives. *Int Immunopharmacol*. 2023;114:109545. doi:10.1016/j.intimp.2022.109545
2. Le Berre C, Honap S, Peyrin-Biroulet L. Ulcerative colitis. *Lancet*. 2023;402(10401):571–584. doi:10.1016/S0140-6736(23)00966-2
3. Gros B, Kaplan GG. Ulcerative colitis in adults: a review. *JAMA*. 2023;330(10):951–965. doi:10.1001/jama.2023.15389
4. Mikami Y, Tsunoda J, Suzuki S, Mizushima I, Kiyohara H, Kanai T. Significance of 5-aminosalicylic acid intolerance in the clinical management of ulcerative colitis. *Digestion*. 2023;104(1):58–65. doi:10.1159/000527452
5. Beiranvand M. A review of the biological and pharmacological activities of mesalazine or 5-aminosalicylic acid (5-ASA): an anti-ulcer and anti-oxidant drug. *Inflammopharmacology*. 2021;29(5):1279–1290. doi:10.1007/s10787-021-00856-1
6. Xu S, He Y, Lin L, Chen P, Chen M, Zhang S. The emerging role of ferroptosis in intestinal disease. *Cell Death Dis*. 2021;12(4):289. doi:10.1038/s41419-021-03559-1
7. Jiang X, Stockwell BR, Conrad M. Ferroptosis: mechanisms, biology and role in disease. *Nat Rev mol Cell Biol*. 2021;22(4):266–282. doi:10.1038/s41580-020-00324-8
8. Ji W, Zhang Y, Qian X, Hu C, Huo Y. Palmatine alleviates inflammation and modulates ferroptosis against dextran sulfate sodium (DSS)-induced ulcerative colitis. *Int Immunopharmacol*. 2024;143(2):113396. doi:10.1016/j.intimp.2024.113396
9. Peng G, Wang S, Zhang H, et al. Tremella aurantialba polysaccharides alleviate ulcerative colitis in mice by improving intestinal barrier via modulating gut microbiota and inhibiting ferroptosis. *Int J Biol Macromol*. 2024;281(4):135835. doi:10.1016/j.ijbiomac.2024.135835
10. Xu M, Tao J, Yang Y, et al. Ferroptosis involves in intestinal epithelial cell death in ulcerative colitis. *Cell Death Dis*. 2020;11(2):86. doi:10.1038/s41419-020-2299-1
11. Liang J, Wang N, Yao Y, et al. NEDD4L mediates intestinal epithelial cell ferroptosis to restrict inflammatory bowel diseases and colorectal tumorigenesis. *J Clin Invest*. 2024.
12. Chen Q, Qiao J, Cao M, Han Z, Zeng X, Zhang X. Spore germinator-loaded polysaccharide microspheres ameliorate colonic inflammation and tumorigenesis through remodeling gut microenvironment. *Mater*. 2023;63:32–49.
13. Ahn JH, Da SPM, Lopez LR, et al. Intestinal E. coli-produced yersiniabactin promotes profibrotic macrophages in Crohn's disease. *Cell Host Microbe*. 2024;33:71–88.
14. Li W, Ding J, Chen S, et al. Alleviation of colitis by honeysuckle MIR2911 via direct regulation of gut microbiota. *J Control Release*. 2024;376:123–137. doi:10.1016/j.jconrel.2024.09.050
15. Wang X, Fang Y, Liang W, et al. Fusobacterium nucleatum facilitates anti-PD-1 therapy in microsatellite stable colorectal cancer. *Cancer Cell*. 2024;42(10):1729–1746.e8. doi:10.1016/j.ccell.2024.08.019

16. Pan X, Shen Q, Zhang C, et al. Coicis semen for the treatment of malignant tumors of the female reproductive system: a review of traditional Chinese medicinal uses, phytochemistry, pharmacokinetics, and pharmacodynamics. *Front Pharmacol*. 2023;14:1129874. doi:10.3389/fphar.2023.1129874
17. Chiang YF, Chung CP, Lin JH, et al. (Coix lacryma-jobi L. var Ma-Yuen Stapf.) ethanolic extract fractions and subfractions induce cell cycle arrest and apoptosis in human breast and cervical cancer cell lines. *Molecules*. 2022;27:13. doi:10.3390/molecules27133984
18. Saez A, Herrero-Fernandez B, Gomez-Bris R, Sanchez-Martinez H, Gonzalez-Granado JM. Pathophysiology of inflammatory bowel disease: innate immune system. *Int J mol Sci*. 2023:24:1526.
19. Mitsialis V, Wall S, Liu P, et al. Single-cell analyses of colon and blood reveal distinct immune cell signatures of ulcerative colitis and crohn's disease. *Gastroenterology*. 2020;159(2):591–608.e10. doi:10.1053/j.gastro.2020.04.074
20. Xu Y, Shen J, Ran Z. Emerging views of mitophagy in immunity and autoimmune diseases. *Autophagy*. 2020;16(1):3–17. doi:10.1080/15548627.2019.1603547
21. Guo M, Du X, Wang X. Inhibition of ferroptosis: a new direction in the treatment of ulcerative colitis by traditional Chinese medicine. *J Ethnopharmacol*. 2024;324:117787. doi:10.1016/j.jep.2024.117787
22. Deng X, Lin B, Wang F, Xu P, Wang N. Mangiferin attenuates osteoporosis by inhibiting osteoblastic ferroptosis through Keap1/Nrf2/SLC7A11/GPX4 pathway. *Phytomedicine*. 2024;124:155282. doi:10.1016/j.phymed.2023.155282
23. Yang J, Liu Y, Lu S, et al. Coix seed oil regulates mitochondrial functional damage to induce apoptosis of human pancreatic cancer cells via the PTEN/PI3K/AKT signaling pathway. *Mol Biol Rep*. 2022;49(7):5897–5909. doi:10.1007/s11033-022-07371-8
24. Jinnouchi M, Miyahara T, Suzuki Y. Coix seed consumption affects the gut microbiota and the peripheral lymphocyte subset profiles of healthy male adults. *Nutrients*. 2021;13(11):4079. doi:10.3390/nu13114079
25. Hu Y, Zhou Q, Liu T, Liu Z. Coixol suppresses NF-kappaB, MAPK pathways and NLRP3 inflammasome activation in lipopolysaccharide-induced RAW 264.7 cells. *Molecules*. 2020;25(4):894. doi:10.3390/molecules25040894
26. Chen L, Shao J, Luo Y, et al. An integrated metabolism in vivo analysis and network pharmacology in UC rats reveal anti-ulcerative colitis effects from Sophora flavescens EtOAc extract. *J Pharm Biomed Anal*. 2020;186:113306. doi:10.1016/j.jpba.2020.113306
27. Wu T, Hu E, Xu S, et al. clusterProfiler 4.0: a universal enrichment tool for interpreting omics data. *Innovation*. 2021;2(3):100141.
28. Gustavsson EK, Zhang D, Reynolds RH, Garcia-Ruiz S, Ryten M. ggtranscript: an R package for the visualization and interpretation of transcript isoforms using ggplot2. *Bioinformatics*. 2022;38(15):3844–3846. doi:10.1093/bioinformatics/btac409
29. Robin X, Turck N, Hainard A, et al. pROC: an open-source package for R and S+ to analyze and compare ROC curves. *BMC Bioinf*. 2011;12:77. doi:10.1186/1471-2105-12-77
30. Engebretsen S, Bohlin J. Statistical predictions with glmnet. *Clin Clin Epigenet*. 2019;11(1):123. doi:10.1186/s13148-019-0730-1
31. Powers RK, Goodspeed A, Pielke-Lombardo H, Tan AC, Costello JC. GSEA-InContext: identifying novel and common patterns in expression experiments. *Bioinformatics*. 2018;34(13):i555–i564. doi:10.1093/bioinformatics/bty271
32. Zhang Z. Reshaping and aggregating data: an introduction to reshape package. *Ann Transl Med*. 2016;4(4):78. doi:10.3978/j.issn.2305-5839.2016.01.33
33. Carpenter CM, Frank DN, Williamson K, et al. tidyMicro: a pipeline for microbiome data analysis and visualization using the tidyverse in R. *BMC Bioinf*. 2021;22(1):41. doi:10.1186/s12859-021-03967-2
34. Zeng X, Wang S, Peng Z, et al. Rapid screening and sensing of stearoyl-CoA desaturase 1 (SCD1) inhibitors from ginger and their efficacy in ameliorating non-alcoholic fatty liver disease. *J Food Meas Charact*. 2024;18(8):6843–6857.
35. Horowitz A, Chanez-Paredes SD, Haest X, Turner JR. Paracellular permeability and tight junction regulation in gut health and disease. *Nat Rev Gastroenterol Hepatol*. 2023;20(7):417–432. doi:10.1038/s41575-023-00766-3
36. Schlegel N, Boerner K, Waschke J. Targeting desmosomal adhesion and signalling for intestinal barrier stabilization in inflammatory bowel diseases-Lessons from experimental models and patients. *Acta Physiol*. 2021;231(1):e13492. doi:10.1111/apha.13492
37. Yang Y, Wang Y, Zhao L, et al. Chinese herbal medicines for treating ulcerative colitis via regulating gut microbiota-intestinal immunity axis. *Chin Herb Med*. 2023;15(2):181–200. doi:10.1016/j.chmed.2023.03.003
38. AlAmeel T, AlMutairdi A, Al-Bawardy B. Emerging therapies for ulcerative colitis: updates from recent clinical trials. *Clin Exp Gastroenterol*. 2023;16:147–167. doi:10.2147/CEG.S375969
39. Lv Q, Xing Y, Liu J, et al. Lonicerin targets EZH2 to alleviate ulcerative colitis by autophagy-mediated NLRP3 inflammasome inactivation. *Acta Pharm Sin B*. 2021;11(9):2880–2899.
40. Qi L, Chen Z, Wang D, et al. Structural characterization of red yeast rice-derived polysaccharide and its promotion of lipid metabolism and gut function in high-fat diet-induced mice. *Int J Biol Macromol*. 2024;282(1):136744. doi:10.1016/j.ijbiomac.2024.136744
41. Zhang Y, Chai N, Wei Z, et al. YYFZBJS inhibits colorectal tumorigenesis by enhancing tregs-induced immunosuppression through HIF-1alpha mediated hypoxia in vivo and in vitro. *Phytomedicine*. 2022;98:153917. doi:10.1016/j.phymed.2021.153917
42. Sui H, Zhang L, Gu K, et al. YYFZBJS ameliorates colorectal cancer progression in Apc(Min/+) mice by remodeling gut microbiota and inhibiting regulatory T-cell generation. *Cell Commun Signal*. 2020;18(1):113. doi:10.1186/s12964-020-00596-9
43. Zhang P, Meng X, Tang X, Ren L, Liang J. The effect of a coix seed oil injection on cancer pain relief. *Support Care Cancer*. 2019;27(2):461–465. doi:10.1007/s00520-018-4313-z
44. Huang X, Wang J, Lin W, et al. Kanglaite injection plus platinum-based chemotherapy for stage III/IV non-small cell lung cancer: a meta-analysis of 27 RCTs. *Phytomedicine*. 2020;67:153154. doi:10.1016/j.phymed.2019.153154
45. Wang Y, Zhang C, Zhang S, et al. Kanglaite sensitizes colorectal cancer cells to Taxol via NF-kappaBeta inhibition and connexin 43 upregulation. *Sci Rep*. 2017;7(1):1280. doi:10.1038/s41598-017-01480-2
46. Xu Q, Kong H, Ren S, et al. Coix seed oil alleviates synovial angiogenesis through suppressing HIF-1alpha/VEGF-A signaling pathways via SIRT1 in collagen-induced arthritis rats. *Chin Med*. 2023;18(1):119. doi:10.1186/s13020-023-00833-6
47. Ye Y, Liu L, Feng Z, et al. The ERK-cPLA2-ACSL4 axis mediating M2 macrophages ferroptosis impedes mucosal healing in ulcerative colitis. *Free Radic Biol Med*. 2024;214:219–235. doi:10.1016/j.freeradbiomed.2024.02.016
48. Li J, Cao F, Yin HL, et al. Ferroptosis: past, present and future. *Cell Death Dis*. 2020;11(2):88. doi:10.1038/s41419-020-2298-2
49. Yu FF, Zuo J, Wang M, et al. Selenomethionine alleviates T-2 toxin-induced articular chondrocyte ferroptosis via the system Xc(-)/GSH/GPX4 axis. *Ecotoxicol Environ Saf*. 2024;290:117569. doi:10.1016/j.ecoenv.2024.117569

50. Cao F, Luo A, Yang C. G6PD inhibits ferroptosis in hepatocellular carcinoma by targeting cytochrome P450 oxidoreductase. *Cell Signal*. 2021;87:110098. doi:10.1016/j.cellsig.2021.110098
51. Yang J, Pei G, Sun X, et al. RhoB affects colitis through modulating cell signaling and intestinal microbiome. *Microbiome*. 2022;10(1):149. doi:10.1186/s40168-022-01347-3